On the evolution of the oceanic component of the IPSL climate models from CMIP3 to CMIP5: A mean state comparison

Juliette Mignot, Didier Swingedouw, Julie Deshayes, Olivier Marti, Claude Talandier, Roland Séférian, Matthieu Lengaigne, Gurvan Madec

Ocean Modelling 72 (2013) 167–184

Contents lists available at ScienceDirect

Ocean Modelling

journal homepage: www.elsevier.com/locate/ocemod

On the evolution of the oceanic component of the IPSL climate models from CMIP3 to CMIP5: A mean state comparison

J. Mignot [a,b,*], D. Swingedouw [c], J. Deshayes [d], O. Marti [c], C. Talandier [d], R. Séférian [c,e], M. Lengaigne [a], G. Madec [a]

[a] LOCEAN/IPSL, UPMC/CNRS/IRD/MNHN, Paris, France
[b] Climate and Environmental Physics, Physics Institute, and Oeschger Centre of Climate Change Research, University of Bern, Switzerland
[c] LSCE/IPSL, CEA/CNRS/UVSQ, Gif-sur-Yvette, France
[d] LPO, CNRS/IRD/UBO/IFREMER, Plouzané, France
[e] CNRM-GAME (Météo-France/CNRS), Toulouse, France

ARTICLE INFO

Article history:
Received 23 March 2013
Received in revised form 4 September 2013
Accepted 7 September 2013
Available online 25 September 2013

Keywords:
Ocean modelling
Parameterizations
Climate model
Coupled ocean biogeochemistry

ABSTRACT

This study analyses the impact on the oceanic mean state of the evolution of the oceanic component (NEMO) of the climate model developed at Institut Pierre Simon Laplace (IPSL-CM), from the version IPSL-CM4, used for third phase of the Coupled Model Intercomparison Project (CMIP3), to IPSL-CM5A, used for CMIP5. Several modifications have been implemented between these two versions, in particular an interactive coupling with a biogeochemical module, a 3-band model for the penetration of the solar radiation, partial steps at the bottom of the ocean and a set of physical parameterisations to improve the representation of the impact of turbulent and tidal mixing. A set of forced and coupled experiments is used to single out the effect of each of these modifications and more generally the evolution of the oceanic component on the IPSL coupled models family. Major improvements are located in the Southern Ocean, where physical parameterisations such as partial steps and tidal mixing reinforce the barotropic transport of water mass, in particular in the Antarctic Circumpolar Current) and ensure a better representation of Antarctic bottom water masses. However, our analysis highlights that modifications, which substantially improve ocean dynamics in forced configuration, can yield or amplify biases in coupled configuration. In particular, the activation of radiative biophysical coupling between biogeochemical cycle and ocean dynamics results in a cooling of the ocean mean state. This illustrates the difficulty to improve and tune coupled climate models, given the large number of degrees of freedom and the potential compensating effects masking some biases.

1. Introduction

A major task in simulating a realistic climate system relies on the development of an accurate ocean model. Indeed, by transporting heat poleward, the "real world" ocean circulation and its thermal properties (large thermal inertia as compared to the atmosphere) play an important role in regulating the earth's mean climate and its variability at millennium (e.g. Clarke et al., 2002, Rahmstorf, 2002), decadal (e.g. Delworth and Mann, 2000; Dijkstra et al., 2006; Kerr, 2000) and interannual (e.g. Swingedouw et al., 2012) timescales. Despite many decades of research, ocean general circulation models (OGCMs) still yield solutions that can substantially deviate from observed ones (e.g. Griffies et al., 2009; Downes et al., 2011), even in terms of mean state. Such deviations have, as a matter of fact, important implications for understanding the present climate and its response to anthropogenic forcing. When an OGCM is coupled to other climatic components, in particular an atmospheric model, tuning is an additional issue.

Climate modelling activity at Institut Pierre Simon Laplace (IPSL) has been in constant evolution since the seminal version of the climate model, developed by Braconnot et al. (1997). Recently, IPSL contributed to the 5th Coupled Model Intercomparison Project (CMIP5) by providing data from its latest version of its coupled model, namely the IPSL-CM5A model. As described by Dufresne et al. (2013), this model, more than a single entity, is a platform that combines a consistent suite of models with various degrees of complexity, diverse components and processes, and different atmospheric resolutions. The aim of the present paper is to detail the formulation of the oceanic component of the climate model

* Corresponding author at: LOCEAN/IPSL, UPMC/CNRS/IRD/MNHN, Paris, France. Tel.: +41 31 631 4275; fax: +41 31 631 8742.
E-mail address: juliette.mignot@locean-ipsl.upmc.fr (J. Mignot).

1463-5003
http://dx.doi.org/10.1016/j.ocemod.2013.09.001

developed at IPSL, and to give insights on its evolution from the IPSL-CM4 version (Marti et al., 2010), used for the 3rd Coupled Model Intercomparison Project (CMIP3), to IPSL-CM5A (Dufresne et al., 2013), used for the 5th (CMIP5).

Both the oceanic and atmospheric components have significantly evolved from IPSL-CM4 to IPSL-CM5A. The atmospheric component is the LMDZ model (Hourdin et al., 2006, 2012). The oceanic component of both versions of the coupled model (IPSL-CM4 and IPSL-CM5A) is the global Océan Parallèlisé (OPA) ocean general circulation model (OGCM), which evolved from OPA8 (Madec et al., 1999) to NEMOv3.2 (Madec, 2008). This change of versions has been accompanied by several modifications and physical parameterizations, in particular the inclusion of a partial step formulation of bottom topography and changes in the vertical mixing scheme. Furthermore, the latest version of the model includes a state-of-the-art biogeochemical component, simulating space and time varying chlorophyll concentrations, namely the Pelagic Interaction Scheme for Carbon and Ecosystem Studies model, hereafter referred as PISCES model (Aumont and Bopp, 2006). Two-way coupling between the physical and biogeochemical components allows the simulated chlorophyll concentrations to interact with optical properties of the ocean modifying in turn the vertical distribution of radiant heating. Several coupled studies (e.g. Lengaigne et al., 2006; Wetzel et al., 2006; Patara et al., 2012) showed for example that introducing interactive biology acts to warm the surface eastern equatorial Pacific by about 0.5 °C. Slight increase of El Niño Southern Oscillation amplitudes is also suggested (e.g. Lengaigne et al., 2006; Marzeion et al., 2005). Other studies however found a net cooling (Gnanadesikan and Anderson, 2009; Manizza, 2005; Sweeney et al., 2005), induced by a dynamical adjustment of the oceanic circulation. Large changes of opposite sign in some cases between these studies are presumably due to different models, parametrization and experimental set-up. Polar regions have also been shown to be affected by these biophysical feedbacks (Gnanadesikan and Anderson, 2009; Lengaigne et al., 2009; Patara et al., 2012; Wetzel et al., 2006): the surface warming in summer resulting from the spring bloom triggering a reduction of sea-ice thickness and concentration. Manizza (2005) demonstrates that biophysical feedbacks prominently enhances the amplitude of the seasonal cycle of Sea Surface Temperature (SST) and mixed layer depth at the mid and high latitude oceans.

This study aims at assessing the respective influence of the physical parameterization changes from OPA8 to NEMOv3.2 along with the implementation of the interactive biogeochemical module in the coupled system on the mean climate state. Various aspects of the North Atlantic climate variability has been studied in both versions of the model and were shown to be very similar: the atmospheric variability (Msadek and Frankignoul, 2008 Gastineau et al., 2012), multidecadal SST variability (Msadek and Frankignoul, 2008; Persechino et al., 2012 Marini and Frankignoul, 2013) air–sea interactions (Gastineau and Frankignoul, 2011). Bi-decadal energy peak in the North Atlantic is present in both versions (Born and Mignot, 2011; Escudier et al., 2012), although with different mechanisms, as well as in piCtrl_noBio. Extensive comparison of CMIP3 and CMIP5 variability patterns in the Pacific shows that both versions correlate very well with observations (Lengaigne, pers. com.). They are also fairly similar in terms of El Niño-Southern Oscillations characteristics (Bellenger et al., 2013).

Section 2 describes the model configurations and the experiments used for this purpose. Section 3 analyses a series of sensitivity tests with ocean-only simulations while coupled models are analysed in Sections 4 and 5. The effect of implementing the biogeochemical module is firstly analysed separately, as it appears to be very important and sometimes contradictory with previous studies. Conclusions are given in Section 6.

2. Experimental design

2.1. General model description

This study focuses on the outcomes of two sets of simulations, the first one using ocean simulations forced by atmospheric reanalyses while the other ones are coupled to other components of the IPSL earth system model. All simulations use the global Océan Parallèlisé (OPA) ocean general circulation model (OGCM, Madec et al., 1999). This model solves the primitive equations on the Arakawa C grid, with a second order centred finite difference scheme. It assumes the Boussinesq and hydrostatic approximations, the incompressibility hypothesis, and uses a free-surface formulation (Roullet and Madec, 2000). The density is computed from potential temperature, salinity and pressure using the Jacket and McDougall (1995) equation of state. Its global ocean configuration used in both versions of the coupled climate model is known as ORCA2. It has a tripolar, quasi-isotropic grid: a combination of an isotropic Mercator grid south of 20 °N, and a non-geographic quasi-isotropic grid north of it, in which the North Pole singularity is replaced by a line between points in Canada and Siberia. A nominal resolution of 2° at the equator is chosen to which a latitudinal grid refinement of 1/2° is added in the tropics. ORCA2 uses realistic bottom topography and coastlines, derived from Smith and Sandwell (1997) up to 60° of latitude and ETOPO5 elsewhere. The maximum depth of 5000 m is spanned by 31 z-levels ranging from 10 m in thickness in the upper 120 m to a maximum of 500 m at the bottom. Vertical mixing is computed from a turbulence closure scheme based on a prognostic vertical turbulent kinetic equation (TKE scheme), which performs well in the tropics (Blanke and Delecluse, 1993). Lateral diffusivity is parameterized by an iso-neutral Laplacian operator with an eddy diffusivity coefficient of 2,000 $m^2\,s^{-1}$. In addition a bolus velocity is applied on temperature and salinity (Gent and McWilliams, 1990) with the NEMO default of a spatially and temporally varying coefficient (calculated from the local growth rate of baroclinic instability and, between 20°N and 20°S, forced to decrease to vanish at the Equator), as described in Treguier et al. (1997). Lateral viscosity is parameterized by a horizontal laplacian operator and an eddy viscosity coefficient of $4.10^4\ m^2\,s^{-1}$ except in the tropics where it reduces to $2.10^3\ m^2\,s^{-1}$ (except along western boundaries) (). The ocean model is coupled to the LIM-2 sea-ice model (Timmermann et al., 2005), which is unchanged in all simulations considered in this study.

In spite of these common aspects, IPSL-CM4 and IPSL-CM5A ocean component has evolved from OPA8 (Madec et al., 1999) to NEMOv3.2 (Madec, 2008) respectively, which implies the implementation of several additional parameterizations related to bottom topography and vertical mixing, as described in the following section, as well as the use of a state-of-the-art biological model, PISCES. The PISCES model is derived from the Hamburg Model of Carbon Cycle version 5 (HAMOCC5) (Aumont et al., 2003). A detailed description of the model parameterizations can be found in Séférian et al. (2012).

The coupled simulations combine the OPA oceanic component to the LMDZ4 (Hourdin et al., 2006) for IPSL-CM4 or LMDZ5A atmospheric model (Hourdin et al., 2012) for IPSL-CM5A. Evolutions between these two models are described in detail in Hourdin et al., 2012). In terms of resolution, given the increasing recognition of the role of the stratosphere in controlling some aspects of the tropospheric climate (e.g. Nikulin and Lott, 2010), priority has been given to vertical resolution increase (from 19 to 39 levels) rather than horizontal resolution. Furthermore, preliminary studies on the atmospheric model have shown that increasing the latitudinal resolution leads to a poleward shift of the jet in the model (e.g. Guemas and Codron, 2011), thereby correcting a major bias of

the IPSL-CM4 model version (e.g. Marti et al., 2010). The atmospheric horizontal resolution has thus been slightly increased from 96×71 grid points ($3.75° \times 2.5°$) in IPSL-CM4 to 96×96 ($1.9° \times 3.8°$) grid points in IPSL-CM5A-LR. The ORCHIDEE model (Krinner et al., 2005) is the land component of the IPSL system. The INCA (INteraction between Chemistry and Aerosol, e.g. Szopa et al., 2012) model is used to simulate tropospheric greenhouse gases and aerosol concentrations, while stratospheric ozone is modelled by REPROBUS (Reactive Processes Ruling the Ozone Budget in the Stratosphere, Lefèvre et al., 1994; Lefèvre et al., 1998).

To conclude, the control simulation of the IPSL-CM4 (Marti et al., 2010) and IPSL-CM5A (Dufresne et al., 2013) models which contributed to the CMIP3 and CMIP5 respectively (hereafter CM4_piCtrl and CM5_piCtrl respectively) differ more than just through the physical parameterizations of their oceanic component. In particular, they also differ in the version and resolution of the atmospheric model they use as well as the inclusion or not of the biogeochemical model. For this reason, it is difficult to compare these simulations directly, and several sensitivity simulations were performed, in forced and coupled mode (Table 1), as described below.

2.2. Experimental setup to assess the impact of physical parameterization changes

A series of experiments in forced mode are first performed, in order to quantify the respective influence of each of the parameterization changes of the oceanic component of the IPSL climate model from IPSL-CM4 to IPSL-CM5A. Table 1 (top) summarizes the five configurations (labelled F1_CMIP3, F2, F3, F4 and F5_CMIP5 respectively) under investigation here. In all these simulations, a sea surface salinity restoring term has been added, with a piston velocity of −166 mm/day as described in Griffies et al. (2009). All forced simulations described here have been integrated for 1500 years under the CORE climatological forcing described in Griffies et al. (2009).

The first major evolution (implemented in F2) relies in the inclusion of a partial step formulation of bottom topography instead of a full step one (Barnier et al., 2006; Le Sommer et al., 2009; Penduff et al., 2007). Indeed, as discussed in Pacanowski and Gnanadesikan (1998) for example, discretizing the bottom topography by steps often leads to a misrepresentation of a gradually sloping bottom and to large localised depth gradients associated with large localised vertical velocities. The partial step formulation improves the representation of bottom bathymetry in ocean models with coarse horizontal and vertical resolution. This development ensures consequently a more realistic flow of dense water mass and their movement associated to the friction along weak topographic slopes (e.g. Pacanowski and Gnanadesikan, 1998).

The second major change, accounted for in F3, is the addition, on top of the 10^{-5} m^2/s background vertical mixing, of a parameterization of the diapycnal mixing associated with the dissipation of internal tides (Simmons, 2004). The additional mixing is inversely proportional to the buoyancy frequency and proportional to the energy transfer from barotropic to baroclinic tides inferred from a tidal model (Carrère and Lyard, 2003). Its vertical structure is a bottom intensified exponential profile with an e-folding scale of 500 m. In Indonesian seas, Simmons (2004) parametrization is replaced by the one proposed specifically for semi enclosed seas by Koch-Larrouy et al. (2007). The latter has been shown to improve water masses characteristics in this area (Koch-Larrouy et al., 2008a,b) and to significantly impact the climate simulated by global coupled GCMs (Koch-Larrouy et al., 2009). Concretely, using results from tidal models, this parametrization provides a four-dimensional (space and time) varying vertical tidal diffusivity, which is added to the vertical mixing in the semi-enclosed seas of the Indian Archipelago.

The third modification deals with improving the surface boundary layer parameterization and light penetration into the ocean and has been implemented in F4. Mixing in the surface boundary layer is based on a Turbulent Kinetic Energy (TKE) scheme (Blanke and Delecluse, 1993) which has been improved as follows (Madec, 2008). First, in mid-latitudes, a small fraction (5%) of the surface input of TKE is enabled to penetrate in the ocean (surface intensified exponential profile with an e-folding scale of 30 m). This change generates mixing below the base of shallow mixed layer in windy condition, and thus improved the mixed layer depth representation in summer below the storm track area. Second, the TKE scheme includes both the effect of Langmuir cell (Axell, 2002) and of surface wave breaking parameterization (Mellor and Blumberg, 2004), and third, the scheme uses a time and space discretization which is energetically consistent with the ocean model equations (Burchard, 2002 Marsaleix et al., 2008). Technical details about these modifications can be found in Madec (2008). Along

Table 1
List of forced and coupled simulations used for this study. The second column describes the evolution of the oceanic numerical code among the different versions, see text for details. The third column gives details on the atmospheric forcing or coupling and the last two columns indicate the initial conditions and the duration of each simulation.

Name of the simulation	Physical characteristics of the ocean	Physical characteristics of the atmosphere	Restart	Duration (yrs)
F1_CMIP3	Std IPSLCM4	CORE climatological forcing	WOA01 Conkright and Boyer (2001) at rest	1500
F2	+partial steps			1500
F3	+kz tides			1500
F4	+vertical mixing improvment, +penetration of the TKE + RGB, + 2D chlorophyll map from SeaWifs,			1500
F5_CMIP5	+ No penetration of the TKE + 3D chlorophyll climatology from PISCES			1500
CM4_piCtrl	As F1_CMIP3, Version used for the CMIP3 (Marti et al. 2010)	LMDZ4 Hourdin et al. (2006), res. 96x71xL19 (Marti et al. 2010)	Several hundreds of years of adjustments	>500
CM5_RETRO	As CM4_piCtrl	LMDZ5A Hourdin et al. (2012), res. 96x95xL39 Dufresne et al. (2013)	WOA Levitus and Boyer (1994) at rest	491
CM5_piStart	As CM5_piCtrl			
CM5_piCtrl_noBio	As CM5_piCtrl without interactive biogeochemistry module. The 3-band penetration scheme Lengaigne et al. (2006) is active.		Yr 1800 of CM5_piCtrl	300
CM5_piCtrl	As F5_CMIP5 + a fully interactive biogeochemistry module Dufresne et al. (2013)		Several hundreds of years of adjustments	>1000

with these mixing parameterization changes, penetration of downward irradiance has also been improved in F4. In F1_CMIP3, F2 and F3, a simple 2-waveband scheme is assumed for the downward irradiance, following Paulson and Simpson (1977). The values of these extinction coefficients correspond to type I water Jerlov, 1968, see also Madec et al., 1999. Such assumption provides a very crude and simplistic representation of observed light penetration profiles (see Morel, 1988). Light absorption in the ocean indeed depends on particle concentration and is spectrally selective. A simplified version of the accurate representation of light penetration using 61 waveband formulation proposed by Morel (1988) was developed by Lengaigne et al. (2006). In this formulation, light is split into three wavebands: blue (400–500 nm), green (500–600 nm) and red (600–700 nm). For each waveband, the chlorophyll-dependent attenuation coefficient is fitted to the coefficients computed from the full spectral model of Morel, 1988) assuming the same power-law relationship. This formulation, called Red–Green–Blue (RGB), reproduces quite closely the light penetration profiles predicted by the 61-wavebands spectral model, but with much greater computational efficiency (Lengaigne et al., 2006). This new spectral model is also included in F4 along with the dependence of light penetration on surface chlorophyll concentration described by SeaWifs observed climatology.

Given the potential bias of the oceanic model, the use of an observed climatology can nevertheless be misleading, so that in the final set up (F5_CMIP5) (the one closest to coupled CM5_piCtrl simulation described below) this observed climatology is replaced by a climatology computed independently with the same oceanic model in forced mode coupled to the biogeochemical model PISCES. Note that the latter is not included interactively in F5_CMIP5, which constitutes an important difference with the oceanic component of the CMIP5 version of the IPSL coupled model. F5_CMIP5 also accounts for all the modifications described above, with the exception of the penetration of turbulent kinetic energy that is not implemented due to flaws in the representation of the SST seasonal cycle. These simulations will be analysed in Section 3.

To test the impact of these physical parameterization changes from OPA to NEMOv3.2 in coupled mode, twin coupled experiments were performed (Table 1, bottom) using the same atmospheric and land surface configurations as CM5_piCtrl (Dufresne et al., 2013), under pre-industrial conditions. The first simulation, CM5_piStart uses also the same oceanic configuration as CM5_piCtrl. The only difference between CM5_piStart and CM5_piCtrl lies in the initial conditions. While CM5_piCtrl results from several hundreds of years of adjustment in coupled and decoupled mode (see Dufresne et al., 2013 for details), CM5_piStart

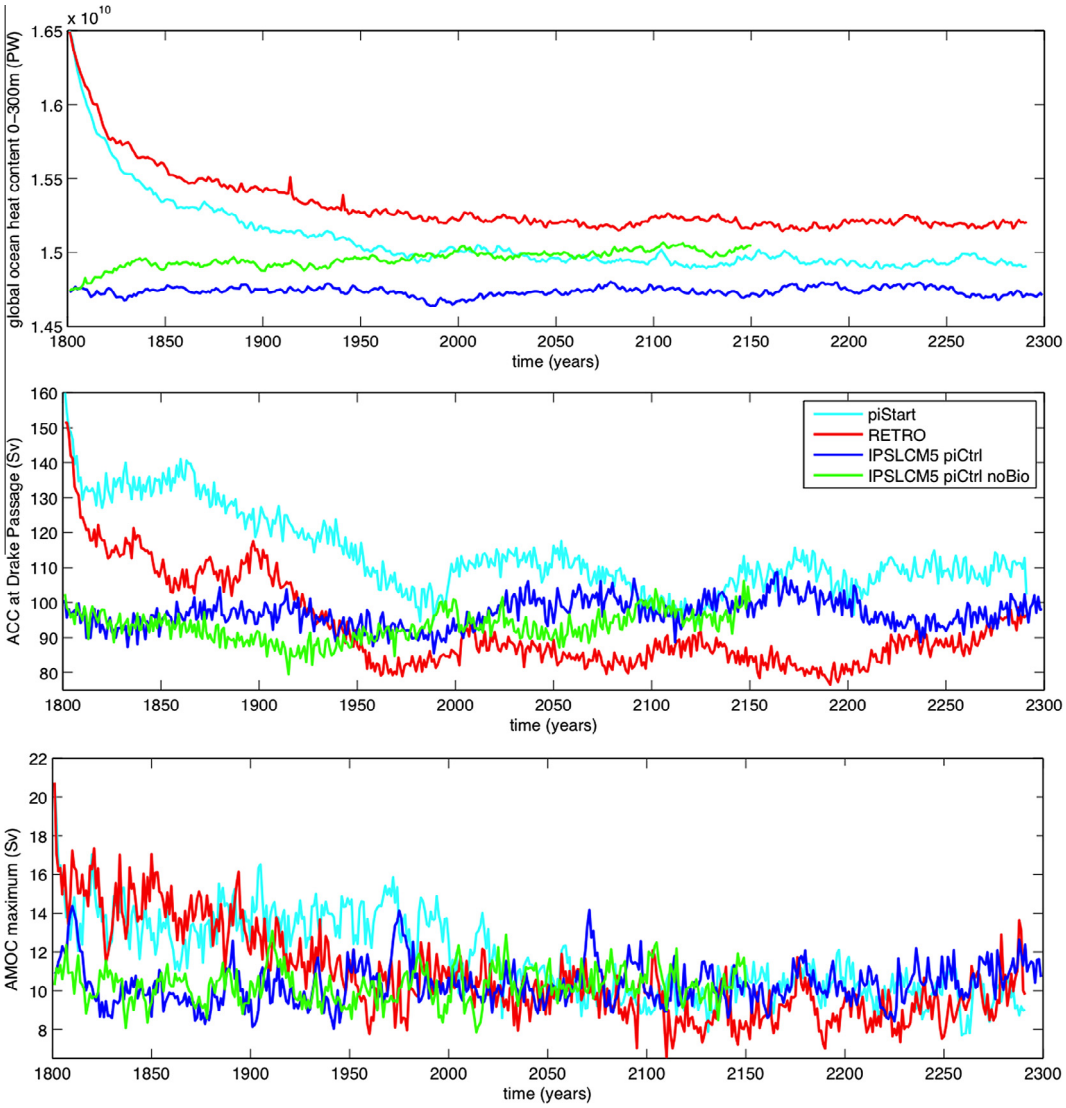

Fig. 1. Top: Globally averaged ocean heat content in the upper 300 m for the three coupled configurations used in the study. Middle: Time series of the barotropic transport at the Drake Passage, bottom: Time series of the Altantic Meridional Streamfunction maximum in the North Altantic.

is started from an ocean at rest using the January temperature and salinity fields from the Levitus World Ocean Atlas (Levitus and Boyer, 1994). In the second experiment, named CM5_RETRO hereafter, the ocean model was set back to the configuration used in IPSL-CM4 (Marti et al., 2010), while the atmospheric and land surface configurations are identical to CM5_piCtrl (and thus CM5_piStart). The coupled simulation CM5_RETRO thus differs from IPSL-CM4 configuration because of evolutions of the atmospheric component, most notably its horizontal and vertical resolutions. This set-up was designed to test the impact of the evolution of the oceanic model on the evolution of the coupled IPSL model. As CM5_piStart, CM5_RETRO was started from the WOA oceanic state at rest, and both these simulations were run for 491 years.

Fig. 1 shows the time series of the global ocean heat content in the upper 300 m (top panel), the total transport integrated over the water column at the Drake Passage (middle panel), and the Atlantic Meridional overturning Circulation (AMOC) maximum (bottom panel) of the three coupled simulations introduced above (red, blue and cyan curves). First of all, although it is clear that the oceanic adjustment requires several hundreds of years, this figure illustrates that all simulations approaches an equilibrium state after 300 years. The latter is nevertheless not reached and may require thousands of years, as it was necessary in CM5_piCtrl. CM5_piStart ends to a globally colder state for the upper ocean than CM5_RETRO, but it is still warmer than the corresponding CM5_piCtrl, further suggesting that the model is not fully equilibrated. The Antarctic circumpolar current (ACC) at Drake Passage is stronger in CM5_piStart than in CM5_RETRO while the magnitudes of the AMOC maximum are similar. These dynamical adjustments will be analysed in Section 5 by comparing the last 92 years of CM5_piStart and CM5_RETRO (yrs 400–491 of these experiments). Given that the two simulations start from the same initial conditions, comparing these relatively short simulations still gives insight in the changes of simulated mean climate.

2.3. Experimental set up to assess the inclusion of the biogeochemical component

To evaluate the effect of the interactive chlorophyll concentration variations related to the inclusion of the biogeochemical component PISCES in IPSL-CM5A as compared to IPSL-CM4 (Section 2a), we performed a sensitivity experiment (called CM5_piCtrl_NoBio) with a set up identical to CM5A_piCtrl, except for the chlorophyll concentration within the ocean which was fixed in time and space to its global mean value of 0.05 mg/m^3 (see Table 1). This value is assumed to be representative to a globally-averaged surface chlorophyll concentration estimated from satellite measurement. This set up aims at evaluating how chlorophyll bio-optical properties impact the ocean thermal structure and circulation. This simulation differs from CM4_piCtrl through the atmospheric and oceanic parameterizations, the atmospheric resolution, but also from the treatment of light penetration into the ocean: the simple 2-waveband scheme assumed for the downward irradiance in IPSL-CM4 is replaced by the RGB formulation described above in both CM5_piCtrl and CM5_piCtrl_noBio simulations. CM5_piCtrl_noBio was run for 350 years, starting from year 1800 in CM5_piCtrl. Differences between these two simulations are described in Section 4. Note that all coupled simulations were run under constant pre-industrial boundary conditions. Furthermore, no specific tuning of the model in general and of the atmosphere in particular was done when plugging the different versions of the oceanic and biogeochemistry model. The tuning is thus identical to CM5_piCtrl.

As displayed on Fig. 1, CM5_piCtrl_noBio (green curve) stabilizes to a warmer global upper ocean state than CM5_piCtrl. Said differently, we detect a cooling in the coupled model after the inclusion of an interactive ocean biogeochemistry. This suggests that the large differences in the upper ocean temperature between IPSL-CM5A and IPSL-CM4 might be understood with the interactive treatment of the marine biogeochemistry. Regarding the dynamics (Fig. 1 middle and bottom panels), though, CM5A_piCtrl_noBio and CM5A_piCtrl do not show strong differences.

3. Oceanic impact of physical parameterization changes in forced mode

Table 2 quantifies the large-scale oceanic circulation response to the successive evolutions introduced in the model set-up. Implementing partial steps intensifies the AMOC by ~2.2 Sv. Implementation of partial steps is indeed known to strengthen the North Atlantic subpolar gyre (Barnier et al., 2006; Myers, 2002), which in turn further intensifies the AMOC intensity through intensified deep convection and increased water column density (e.g. Mellor et al., 1982; Greatbatch et al., 1991; Eden and Willebrand, 2001; Levermann and Born, 2007). Implementation of partial steps also intensifies the ACC by ~10%. This could result directly from an increase in the barotropic circulation through the inclusion of partial steps or indirectly from the intensification of North Atlantic Deep Water (NADW) formation, which contributes to strengthen the density gradient across the ACC in the South Atlantic and thus potentially increases the ACC transport (e.g. Brix and Gerdes, 2003). Adding a tidal mixing parameterization favours an intensification of the formation and circulation of Antarctic Bottom Water (AABW) (simulation F3). Indeed, increasing vertical mixing in vicinity of the bottom this intensification favours the mixing of AABW with the overlying water masses, thereby favouring its formation. Deep convection in the Southern Ocean however primarily takes place unrealistically in the Weddell Sea interior, as in most coarse resolution ocean models (e.g. Griffies et al., 2009). Improved tidal mixing also further strengthens by ~10% the ACC at the Drake Passage, which is likely driven by the intensification of the density gradient across the Southern Ocean associated with the AABW formation increase (Lefebvre et al., 2012). No strong changes occur in F4 and F5_CMIP5 in terms of large-scale oceanic circulation.

Changes in physical parameterizations also alter ocean temperature (Fig. 2) and salinity (not shown) distribution. As compared to the WOA (Fig. 2, bottom row), all simulations exhibit warm anomalies around 40–50°N down to 1000 m. This is related to a persistent bias in the position of the North Atlantic Current, located too far North (e.g. Griffies et al., 2009). F1_CMIP3 also shows a bias in the Southern Ocean, consisting of a positive temperature bias around 100 m centred at 60°N and a negative one below, extending down to more than 1000 m and towards the Equator. Including the representation of partial steps (F2 simulation) further strengthens the cold bias at 1000 m depth while slightly reducing it in the Southern Ocean below 1000 m in response to the intensification of AABW formation and ACC. A similar relationship between the

Table 2
Main dynamical characteristics in the forced ocean simulations. The intensity of the MOC is computed as the maximum of the Atlantic meridional streamfunction at 45°N. The AABW is the minimum of the global meridional streamfunction between 60°S and 80°S and between 500 and 2500 m. The ACC is evaluated as the intensity of the barotropic flow at the Drake Passage. Bold numbers highlight the major effect of the corresponding evolution.

Run	MOC (Sv)	AABW (Sv)	ACC (Sv)	AABW formation (Sv)
F1_CMIP3	13.08	9.51	107.12	5.67
F2	**15.25**	8.48	119.45	5.96
F3	15.97	**13.17**	**129.66**	**7.20**
F4	15.54	12.52	128.8	7.15
F5_CMIP5	16.15	13.03	130.16	7.35

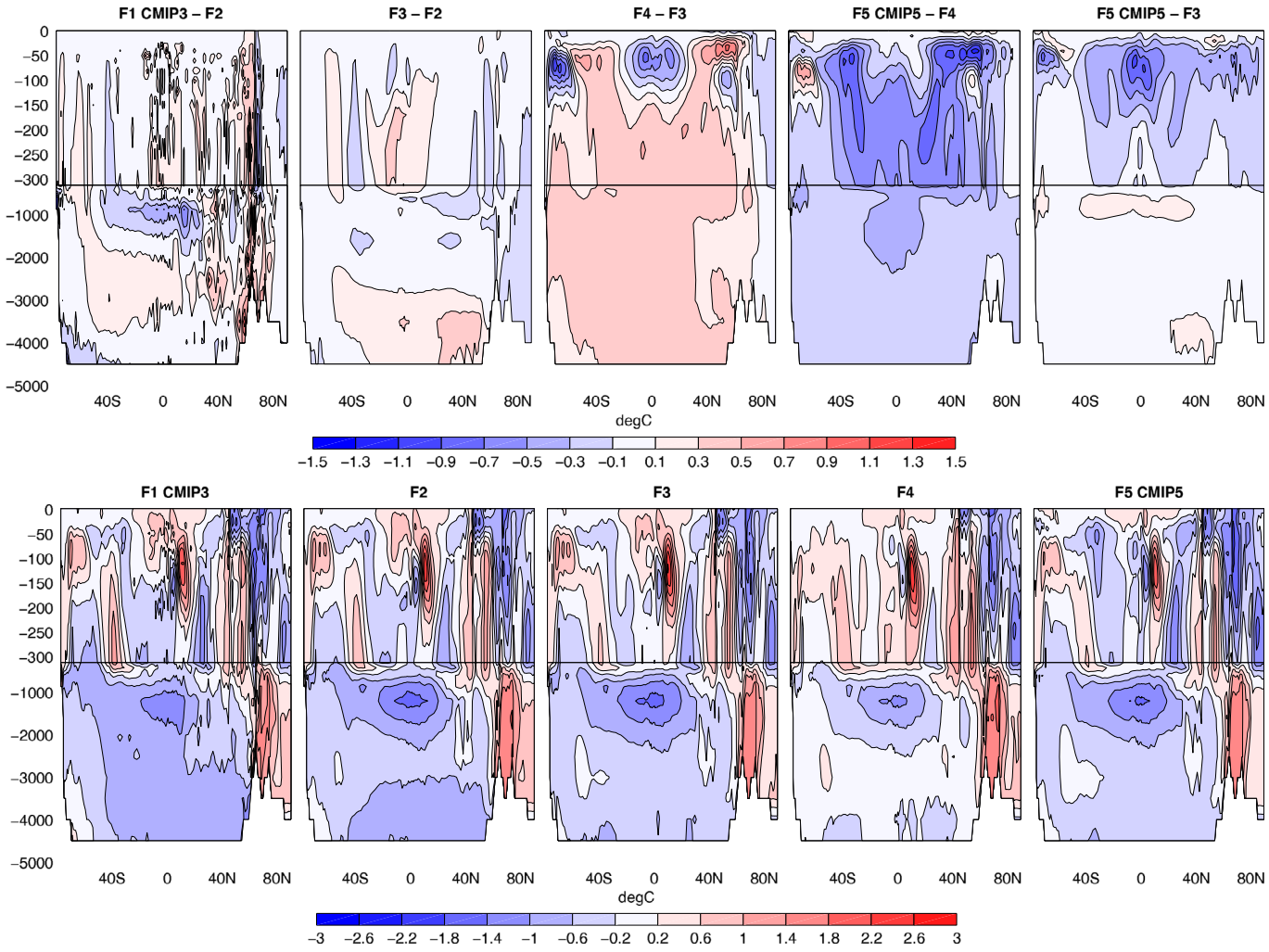

Fig. 2. Top : Successive differences of the zonal mean temperature profiles in the forced oceanic configurations described in Table 1 from F1_CMIP3 (left) to F5_CMIP5 (fourth panel from the left). The last panel on the right shows the difference between F5_CMIP5 and F3, where evolutions mainly concern the inclusion of the RGB model and a 3-dimensional map of chlorophyll. Bottom: Differences to WOA01 of the zonal mean temperature profiles in the forced oceanic configurations described in Table 1. Note that the color scale is doubled in the bottom panel.

intensification of the AABW formation and anomalous warming in the Southern Ocean has been discussed by Swingedouw et al. (2008). The Southern Ocean warming is considerably strenghtened when implementing the new TKE scheme (F4 simulation), bringing the simulation much closer to the observed climatology in this region (Fig. 2). However, accounting for this new parameterisation also unrealistically damps the amplitude of the SST seasonal cycle in particular in the Northern Hemisphere (Fig. 3). This major drawback largely arises from the strong summer surface cooling driven by a deeper mixing penetration. It led to the decision not to include this parameterisation in the final CMIP5 version of the coupled IPSL model. Note that this simulation also includes the new RGB light penetration scheme that presumably drives the anomalous subsurface cooling in the tropics, while warm anomalies at mid-latitudes are most likely driven by changes in the mixed layer physics, as shown below. In the F5_CMIP5 configuration, the new TKE scheme was removed and a modelled 3-dimensional distribution of chlorophyll was used. It remains difficult to decipher the specific effect of each of these modifications. A mid-latitude subsurface cooling largely compensates the warm bias that was detected in F4, highlighting the cancellation of the effect of the new TKE scheme. The upper right panel displays the temperature differences between F5_CMIP5 and F3, which sheds a light on a dominant cooling in the upper 200 m in the tropics and in the upper 400 m in the

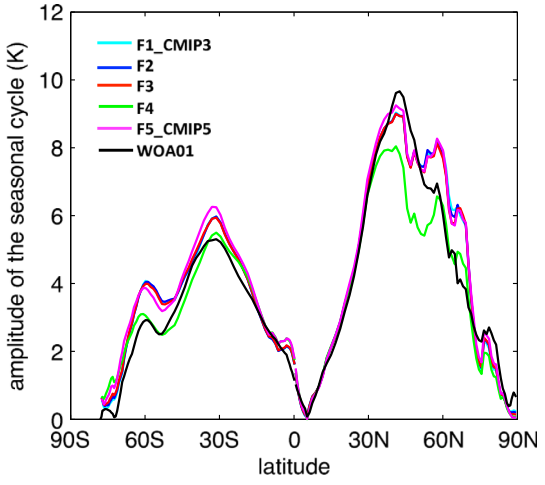

Fig. 3. Amplitude of the seasonal cycle of globally averaged SST in F1_CMIP3 (cyan), F2 (blue), F3 (red), F4 (green) and F5_CMIP5 (magenta), together with observations from the WOA (Levitus and Boyer, 1994). (For interpretation of the references to colour in this figure legend, the reader is referred to the web version of this article.)

subtropics. This cooling is attributable to several modifications in light penetration scheme, precisely the RGB scheme and the 1-dimensional response to biophysical feedback to the light penetration set by a present-day chlorophyll climatology. The impact of interactive biology is further investigated in the following sections.

4. Influence of the interactive biological module in coupled mode

Fig. 4 shows the climatological SST differences between CM5_piCtrl and CM5_piCtrl_noBio. The annual mean SST is colder over most of the globe when using the interactive biogeochemistry module. The effect is weaker and even opposite in eastern equatorial areas and coastal upwelling regions, as well as along western boundary currents at mid-latitudes and Southern and Arctic Oceans while it is strongest in the centre of subtropical gyres. The root mean square averaged SST difference among the two runs amounts 0.14 K.

The one-dimensional thermal adjustment of the ocean to the inclusion of biogeochemistry is expected to induce an anomalous surface warming in CM5_piCtrl as compared to CM5_piCtrl_noBio in eutrophic regions (i.e. in regions where the modelled chlorophyll concentration is higher than 0.05 mg/m^3). Indeed, high chlorophyll concentrations amplify the thermal disequilibrium in the water column by trapping more heat at the surface of the ocean and cooling subsurface waters. The opposite takes place in oligotrophic regions such as the centre of the subtropical gyres. There, the observed chlorophyll concentration, as well as the one simulated in CM5_piCtrl, is lower than 0.05 mg/m^3 (e.g. Séférian et al., 2012). As a result, less heat is trapped in the surface layer in these areas in CM5_piCtrl as compared to CM5_piCtrl_noBio, explaining the cold surface anomalies seen on Fig. 4. Coastal upwellings in equatorial regions, on the other hand, are relatively rich in chlorophyll, and one would expect a net surface warming in CM5_piCtrl as compared to CM5_piCtrl_noBio. This is what is found by Lengaigne et al. (2006) and Patara et al. (2012), two independent studies using similar twin experiments with another coupled climate model and the same oceanic component as ours, namely NEMO. Yet, in our case, the warming effect is very weak or absent (Fig. 4).

At mid to high latitudes, previous studies (e.g. Lengaigne et al., 2009; Manizza, 2005) have suggested that bio-physical feedbacks would result in an intensification of the seasonal cycle: in summer, the presence of phytoplankton increases the surface warming, as more heat is trapped at the ocean surface, while in fall and winter, the deepening of the mixed layer acts to bring the underlying anomalously cold layers to the surface. This is indeed the case in our simulations for the Southern Ocean and the subpolar North Atlantic and North Pacific that are marked by a warming in local summer in CM5_piCtrl (Fig. 4, right panel), and a moderate to strong cooling in winter (Fig. 4, middle panel). Consistently, the seasonal cycle of SST at mid to high latitudes is slightly enhanced in CM5_piCtrl as compared to CM5_piCtrl_noBio (Fig. 5). Note however that the physical parameterization changes described in Table 1 induce much stronger changes to the seasonal cycle amplitude in CM5_piStart compared to CM5_RETRO than to CM5_piCtrl_noBio (Fig. 5). Such effect can hardly be seen in forced mode (Fig. 3) and might thus be due to air-sea interactions. In annual mean (Fig. 4, left), ice-free areas at northern high latitudes experience a cooling in CM5_piCtrl as compared to CM5_piCtrl_noBio, which again differs from earlier studies, in particular Lengaigne et al. (2009). These authors have argued that warming associated to phytoplankton blooms occurs concomitantly with the ice retreat along the Arctic coastal shelves in spring and this mechanism is then amplified in summer due to a larger reduction of sea-ice thickness and concentration. In our model, such biologically-induced warming occurs indeed in summer but its global effect is largely counteracted by the winter cooling.

Fig. 6 shows the adjustment of the model to the biogeochemical component, helping to understand differences with previous model versions: during the first decade (left panel), the anomalous vertical temperature profile is close to what is expected from the one-dimensional adjustment described above, and broadly agrees

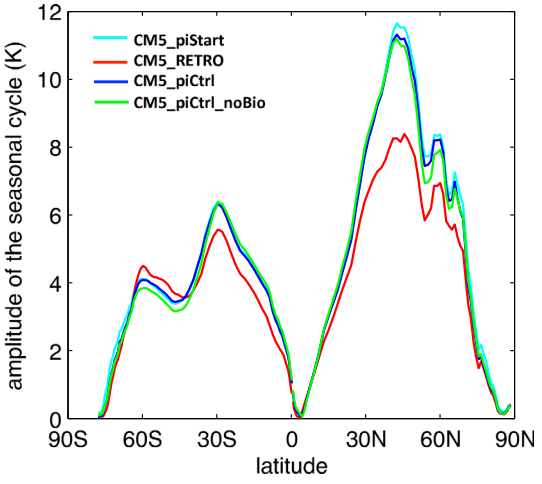

Fig. 5. Amplitude of the seasonal cycle of globally averaged SST in CM5_piStart (cyan), CM5_RETRO (red), CM5_piCtrl (blue) and CM5_piCtrl_noBio (green). (same colour code as Fig. 1). (For interpretation of the references to colour in this figure legend, the reader is referred to the web version of this article.)

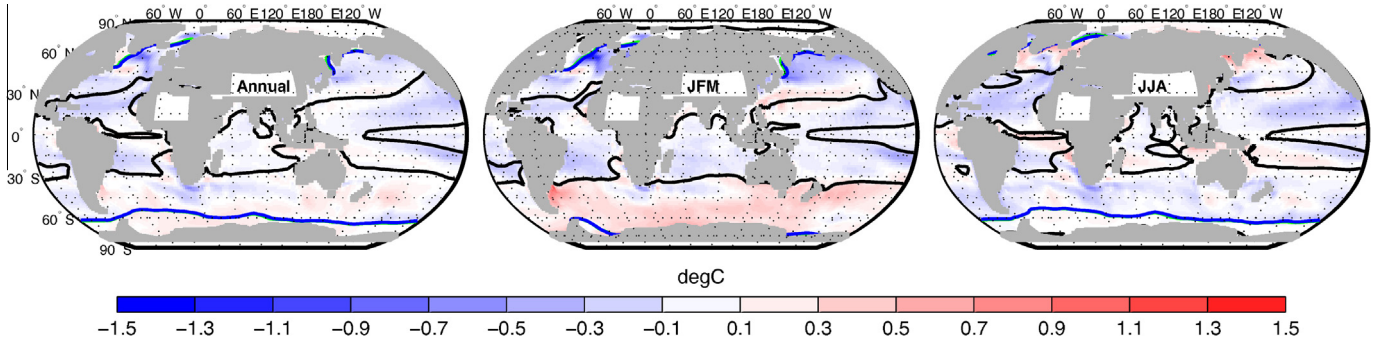

Fig. 4. CM5_piCtrl–CM5_piCtrl_noBio SSt differences computed over [1800–2150] in annual means (left), for the winter season (JFM, middle) and the summer season (JJA, right). The blue line shows the limit of 10% sea ice coverage in CM5_piCtrl during the corresponding season. The green line shows the same for CM5_piCtrl_noBio (note that the two are almost superposed). The black line shows the contour of 0.05 mg/mL of surface chlorophyll concentration in CM5_piCtrl. (For interpretation of the references to colour in this figure legend, the reader is referred to the web version of this article.)

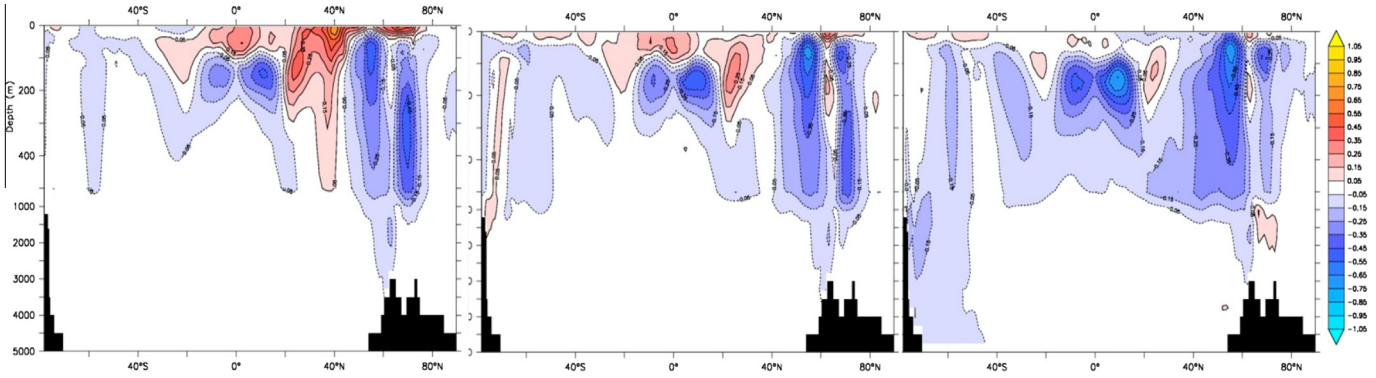

Fig. 6. CM5_piCtrl–CM5_piCtrl_noBio zonal average temperature differences over yrs 0–10(left), 10–20 (middle) and 50–100 (right).

with results from Lengaigne et al. (2006, 2009). Equatorward of 10° of latitude, as well as at high northern latitudes, where the chlorophyll concentration exceeds 0.05 mg/m^3, the surface is anomalously warm and the subsurface anomalously cold when the chlorophyll concentration is interactive as compared to when it is kept at a (lower) constant value. More heat is trapped in surface and thus less heat penetrates into the ocean interior, as found in Lengaigne et al. (2006). The opposite effect takes place in the southern subtropics while the strong warming in the northern subtropics could be due to the specific timing of the phytoplankton bloom in this region in IPSL-CM5A (Séférian et al., 2012). The middle and right panels in Fig. 6 show that this situation evolves after the first decade and the ocean globally becomes colder in CM5_piCtrl than in CM5_piCtrl_noBio. This suggests a delayed adjustment of the ocean overwhelming the direct 1-dimensional effect. This evolution is also seen in each basin taken individually, while the large-scale meridional transport is unchanged, as seen in Fig. 1 (bottom) for the Atlantic. A role of the oceanic circulation and in particular the AMOC in this slow adjustment is thus excluded.

As discussed in Gnanadesikan and Anderson (2009), the net effect detected in these kinds of twin experiments depends on the set-up of the control simulation without interactive biogeochemistry. We indeed found major differences in the chlorophyll vertical distribution, in particular equatorward of 30° of latitude (Fig. 7) between our control run and the one used in Lengaigne et al. (2006), which was very close to CM4_piCtrl. More precisely, concentrations at the surface are similar, but CM5_piCtrl is much poorer than the previous model version between the surface and 150 m depth. This implies that the anomalous warming linked to the capture of light by the chlorophyll is weaker down to 150 m in CM5_piCtrl as compared to Lengaigne et al. (2006). Consistently, photosynthetically available radiation (PAR) is weaker in CM5_piCtrl in upper layers (not shown). This might explain why eventually, in our experiments, subsurface cooling overwhelms surface warming. Differences in the interactive chlorophyll profiles are prominently driven by the vertical distribution of nutrients, the ocean circulation (mixed-layer depth) and the incoming shortwave radiation, since these three parameters control the nutrient-to-light co-limitation of the phytoplankton growth. A quantitative skill assessment of the marine biogeochemistry has been performed with two control simulations of IPSL-CM4 and IPSL-CM5A in Séférian et al. (2012) and with the same forced configuration as F4 in Duteil et al. (2011). These two studies reveal in particular that errors in ocean circulation lead to an unrealistic distribution of nutrients, which in turn impacts the distribution of chlorophyll. These latters impact finally the penetration of the radiant heat, and thus the ocean circulation.

To conclude, including an interactive biology module induced an anomalous surface warming in our coupled model during the

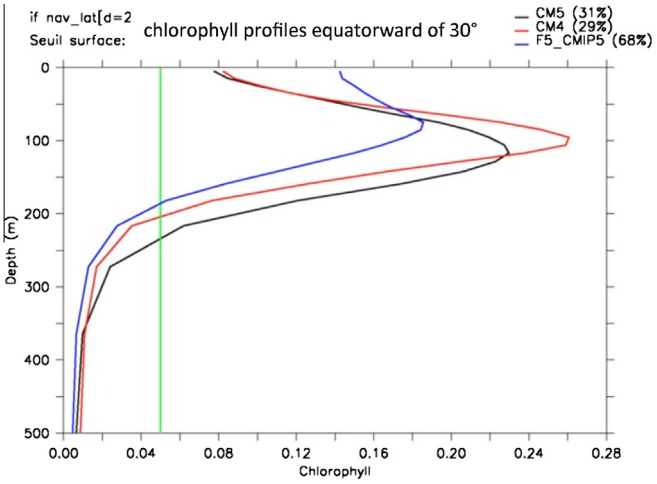

Fig. 7. Vertical distribution of the chlorophyll concentration (in mg/m^3) averaged over all oceanic basins equatorward of 30° of latitude in cM5_piCtrl (black line), the control simulation considered in Lengaigne et al (2006) (red line) and in F5_CMIP5 (blue line). (For interpretation of the references to colour in this figure legend, the reader is referred to the web version of this article.)

first decade but a net global surface cooling on the longer term. Seasonally, though, mid to high latitude oceans do show an anomalous summer warming, in agreement with a 1-dimensional adjustment to the biogeochemical module. The global annual effect thus probably helped to reduce the warm tropical bias described in the previous version of the model by Marti et al. (2010), even if not necessarily for mechanistically correct reasons. On the other hand, it contributed to worsen the cold bias at mid-to high latitudes, which reached 6 °C in the North Atlantic in CM4_piCtrl (Marti et al., 2010) and 8 °C in CM5_piCtrl at the same location, around 50°N. This leads to a large overestimation of the winter sea-ice cover in the Nordic Seas and a reduction of oceanic deep convection in this area in CM5_piCtrl as compared to CM4_piCtrl. This partly explains the degradation of the representation of the deep oceanic overflows across Greenland-Iceland-Scotland ridges (not shown). Note however that, as explained in Marti et al. (2010), this extreme cold bias also results from a combination of a southward shift of the North Atlantic drift due to an equartorward bias of the wind. Indeed, the AMOC and the SST cold bias in the North Atlantic is reduced with increasing atmospheric horizontal resolution, due to reduction of the zonal wind stress bias (*cf.* Dufresne et al. 2013). Note also that specific model tuning could have reduced the surface bias. Such tuning was intentionally not part of this set of experiments to maximise comparability. We also noted that the effect of physical changes on the seasonal cycle of SST is stronger than the biogeochemical effects.

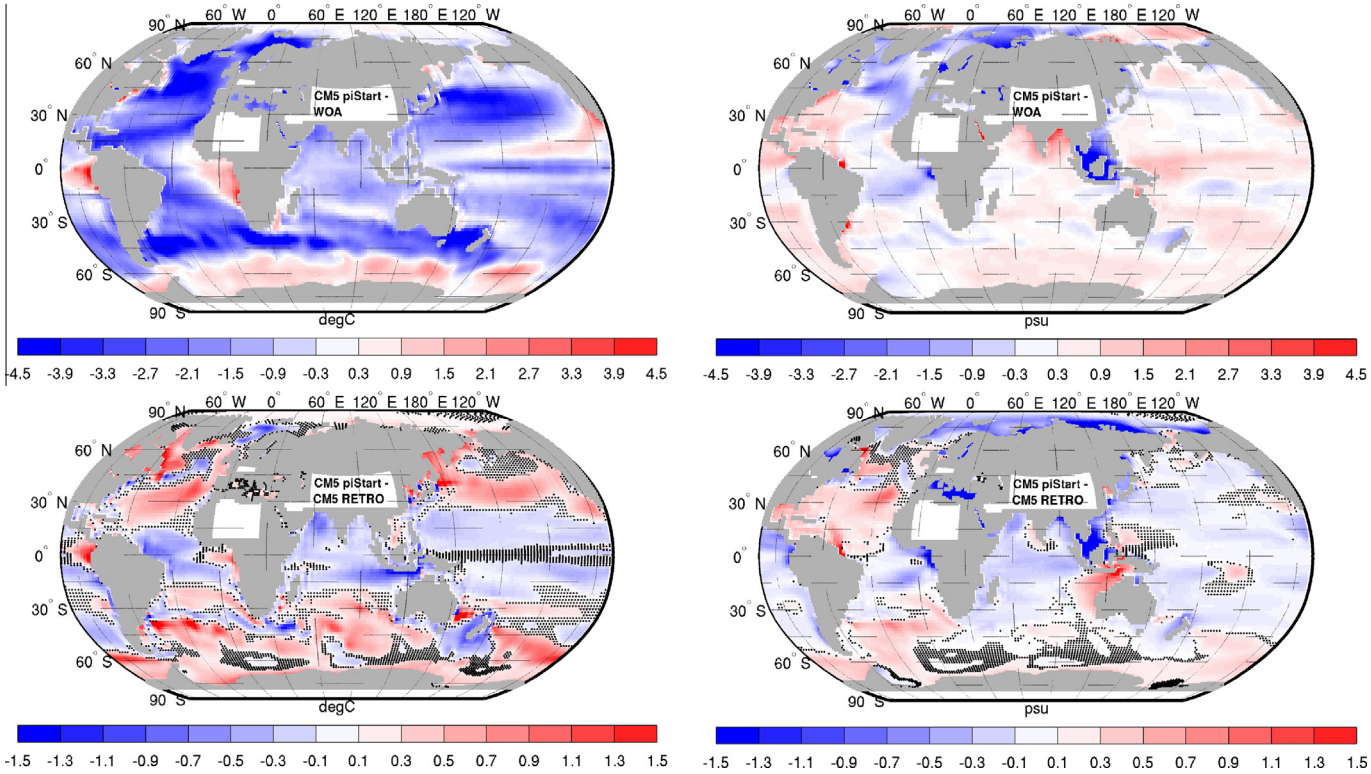

Fig. 8. Annual mean SST (left) and SSS (right) anomalies in CM5_piStart as compared to the WOA (Levitus and Boyer, 1994) (top) and as compared to CM5_RETRO (bottom). All averages are computed over the years [2200–2291] of simulations. Black dots on bottom panels show areas where the differences between the two runs is not significant at the 95% level according to a Student test under the assumption that the variance is unchanged.

5. Evolution of the oceanic component in coupled mode

5.1. Temperature and salinity distribution

Fig. 8 displays the annual mean surface ocean temperature and salinity anomalies in CM5_piStart and CM5_RETRO averaged over the time interval [2200–2291] (last 92 years of the simulations). All following figures are shown for the same time interval. The oceanic surface is generally colder in CM5_piStart than the observations (Fig 9. upper left panel). This cold bias extends down to 500 m, and even deeper in the Southern Ocean (Fig. 9 top left panel). Note however that the WOA data (Levitus and Boyer, 1994) are a synthesis of modern values while all simulations investigated here are driven by preindustrial boundary conditions, with lower radiative forcing than under present days, so that part of this cold bias can be related to this difference in radiative forcing. The cold bias is nevertheless generally stronger in CM5_piCtrl as compared to CM5_piStart by roughly 1 °C (not shown). Notable exceptions are around 40–50°N in the Atlantic and the Pacific: at these locations, where the cold bias in CM5_piStart is maximum (in summer), it exceeds the one found in CM5_piCtrl by about 0.5 °C. These differences further illustrate the fact that CM5_piStart is still drifting, as already seen in Fig. 1.

Differences between CM5_piStart and CM5_RETRO are easier to interpret than differences between CM5_piStart and CM5_piCtrl as the two experiments started from the same initial state and were integrated for equally long. Surface differences (Fig. 8 bottom left) are generally stronger than between CM5_piCtrl and CM5_piCtrl_noBio (compare Fig. 4 left). The root mean squared difference between CM5_piStart and CM5_RETRO in terms of global SST amounts 0.33 °C, which is about three times stronger than between CM5_piCtrl and CM5_piCtrl_noBio. This suggests that changes in dynamical parameterizations have together a stronger effect than the one of interactive biology in the surface layers. Note however that the latter changes the mean state, as seen above, on which the dynamical parameterizations act. It is thus difficult to separate both effects. Furthermore, over the upper 300 m, the root mean square error between CM5_piStart and CM5_RETRO falls down to 0.15 °C, as compared to 0.23 °C between CM5_piCtrl and CM5_piCtrl_noBio. This suggests that the interactive biogeochemical module has a major effect on the upper ocean three-dimensional temperature distribution of the IPSL model. More precisely, the root mean square difference between CM5_piCtrl and CM5_piCtrl_noBio is maximum when the temperature is averaged over the upper 300 m (0.23 °C), suggesting that the main effect of interactive biogeochemistry occurs around 300 m depth.

Ocean mean state resulting from CM5_piStart configuration is colder than that of CM5_RETRO at the surface of tropical and subtropical domains (Fig. 8 bottom left). At mid-latitudes, on the other hand, CM5_piStart configuration leads to a generally warmer oceanic mean state in surface. Below the first layer, oceanic mean state produced by CM5_piStart configuration is colder down to more than 1000 m compared to CM5_RETRO (Fig. 9 bottom left panel). Consistent findings were found in forced models (compared F3 and F5_CMIP5 Fig. 2, right panel), yet reaching slightly shallower depths, and with a more intense cooling in the tropics due to the implementation of the RGB penetration scheme. This scheme is present in both CM5_piStart and CM5_RETRO configurations, so that its effect is not visible here in coupled mode (see Lengaigne et al., 2006 for more details). The subsurface temperature differences between CM5_RETRO and CM5_piStart configurations are largely attributable to the interactive chlorophyll module, as described in Section 4.

We focus now on regional differences between the two simulations. In the North Atlantic, SST differences between CM5_piStart and CM5_RETRO are closely associated to SSS differences (Fig. 8

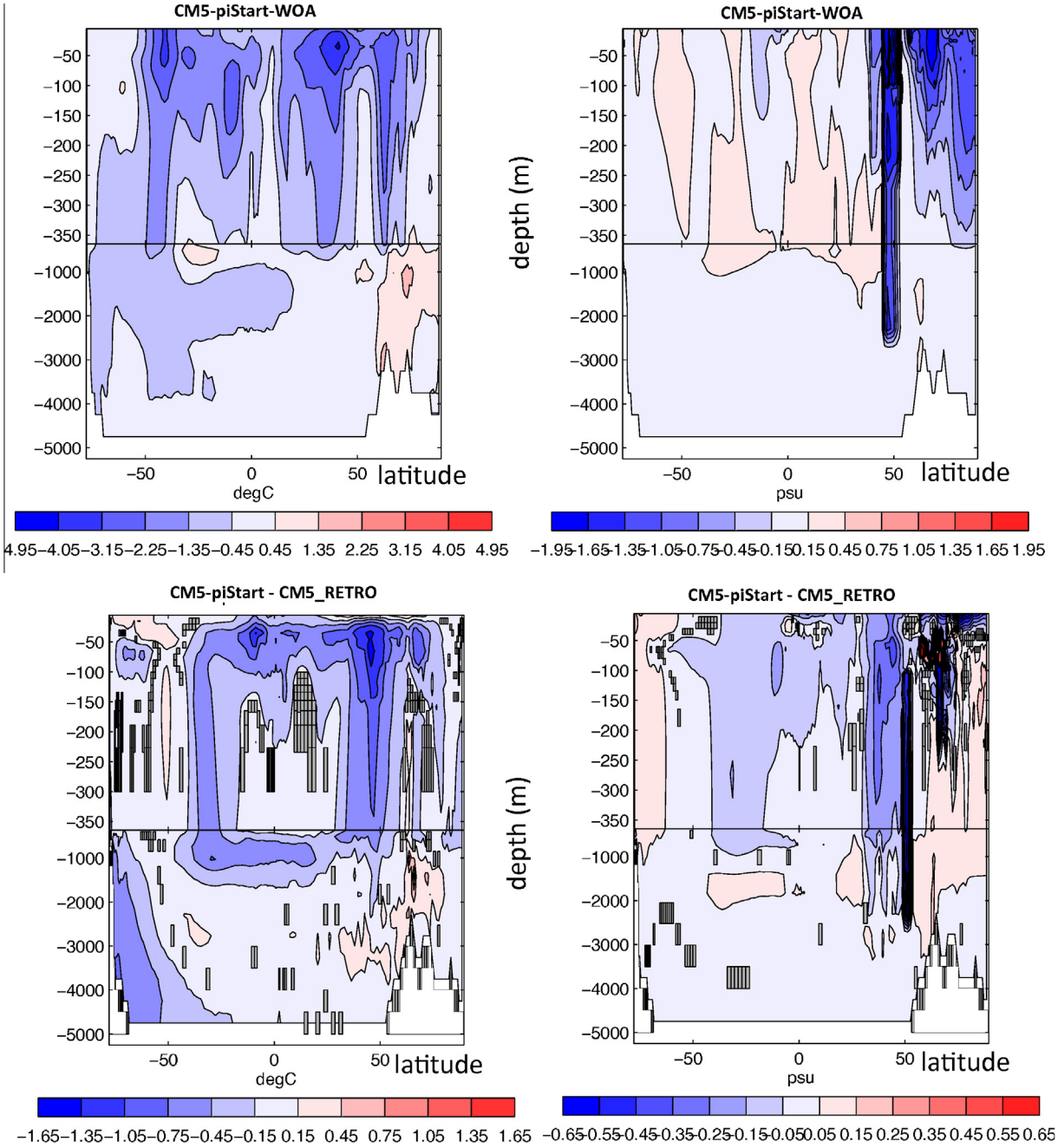

Fig. 9. Annual mean zonal mean temperature (left) and salinity (right) in CM5_piStart as compared to the WOA (top) and as compared to CM5_RETRO (bottom). All averages are computed over the years. [2200–2291] of simulations. Grey shading on bottom panels show areas where the differences the two runs is not significant at the 95% level according to a Student test under the assumption that the variance is unchanged.

bottom right). This suggests a role of the oceanic circulation, bringing more warm and salty waters northward in CM5_piStart. Nevertheless, as described e.g. by Mikolajewicz and Voss (2000), a change of stratification due to the shortwave radiation effect on temperature would modify the mixing and thus also possibly the salinity. The warm anomalies in the North Pacific mid-latitudes are also associated with adjustments of the oceanic circulation. These hypotheses will be demonstrated below.

In the Southern Ocean, CM5_piStart is generally too cold around 50°S and too warm south of 60°S in the surface as compared to observations (Fig. 8 top left). The warm surface anomalies do not extend at depth though, where CM5_piStart is generally too cold over the whole water column (Fig. 9 top left). This surface warm bias remains relatively unchanged in CM5_RETRO. Yet it extends down to almost 1000 m as well as along the oceanic floor (except for weak anomalies of the opposite sign between 50 m and 100 m, suggesting a modification of the thermocline). This is consistent with the forced simulations (compare F5_CMIP5 and F1_CMIP3, Fig. 2). The suite of sensitivity experiments in forced mode suggests that this effect is due to the implementation of the partial steps (F2).

Bottom waters along the Antarctic continental shelf are colder in CM5_piStart as compared to CM5_RETRO. This is indicative of an intensified AABW formation, in agreement with forced simulations, and confirmed by deeper mixed layers (not shown) and meridional streamfunctions (below). Furthermore, along the Antarctic continent, surface water masses are saltier in CM5_piStart, while they are fresher north of 50°S (Fig. 9 bottom right). Fig 10

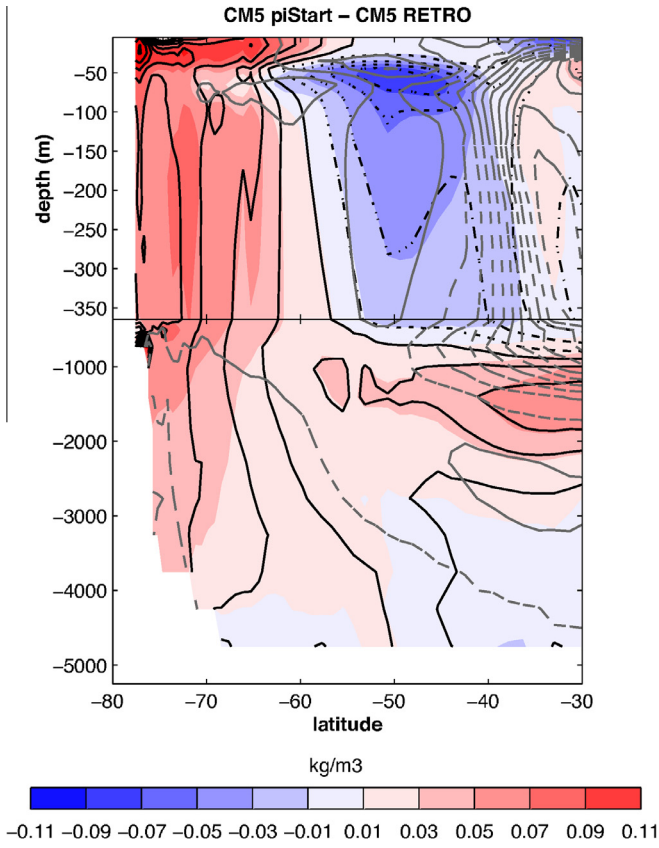

Fig. 10. Annual mean zonal mean potential density difference between CM5_piStart and CM5_RETRo for the years 2200–2291. The black contours show the difference in the linearized haline contribution to density (solid lines for positive difference, dashed line for negative differences, same contour intervals as for density). The grey lines show the temperature differences (same contour interval as for density).

shows that these salinity anomalies in the Southern Hemisphere are responsible for an increase of the density gradient across the Southern Ocean (80°S–50°S) in CM5_piStart by roughly 15% as compared to CM5_RETRO. This consistent with intensified ACC in CM5_piStart, as described below.

Regarding the tropical regions, Fig. 8 (bottom) shows that surface waters are colder by up to 1 °C and saltier by more than 1.5 psu in CM5_piStart as compared to CM5_RETRO in the southern part of the Indonesian Archipelago (IA). This results from the implementation of tidal mixing, consistent with coupled simulations from Koch-Larrouy et al. (2009). Further north, offshore of southeastern Asia, CM5_piStart displays a strong fresh anomaly compared to observations while this anomaly was much weaker in CM5_RETRO. This difference between the two simulations can be partly tracked down to changes in atmospheric freshwater flux, as shown in Fig. 12, with larger precipitation into the ocean (blue colour) in CM5_piStart along 5°N and weaker along the Equator and 5°S in the Indian Ocean. These changes are the signature of a northward shift of the ITCZ, and induce the SSS anomalies seen in Fig. 8 (bottom right). Note that from Fig. 12, atmospheric freshwater changes are also very strong in the tropical Atlantic, similarly characterised by a northward shift of the mean ITCZ position (around 10°N). Stronger precipitation are also found along 10°S. This change of freshwater forcing in the deep tropical band yields fresher surface waters in CM5_piStart as compared to CM5_RETRO in the deep southern tropics of the Atlantic and eastern Indian oceans, and saltier ones in the North, especially around the mouth of the Amazon river. Along 15°N in the Atlantic, however, another process must be invoked to explain the positive salinity anomalies in spite of an increase of freshwater into the ocean. The acceleration of the subtropical gyre and the AMOC at tropical latitudes (see below) transporting salty waters northward is a plausible candidate. Note also that changes in both SSS (Fig. 8 bottom right) and atmospheric freshwater fluxes (Fig. 12 bottom, colours) are much weaker in the tropical Pacific.

A warm bias is detected in the coastal upwelling areas in CM5_piStart Fig. 8 (top left), as in CM4_piCtrl and CM5_piCtrl (not shown). Poor representation of coastal regions and upwelling processes is a typical bias in coupled ocean–atmosphere models (IPCC, Fig. S8.1, Davey et al., 2002). Biases in marine stratus and stratocumulus clouds have been suggested to explain these large SST biases in the Pacific and Atlantic oceans (e.g. Meehl et al., 2005), as well as underestimation of alongshore surface winds by the atmospheric general circulation model (e.g. Huang and Schneider, 1995; Kiehl and Gent, 2004; Braconnot et al., 1997) and coarse oceanic resolution is insufficient to resolve vigorous meso-scale eddies, which spread the cold signals from the coastal upwelling zone of several tens of kilometres into the open ocean (e.g. Penven, 2005). This coastal warm bias is stronger in CM5_piStart than in CM5_RETRO (Fig. 8 bottom left). Reasons for this difference are unclear at this stage. However, as discussed above, this could at least partly be a consequence of the transient adjustment process as this bias is further reduced in CM5_piCtrl. Fig 11 (bottom, colours) shows that associated anomalous atmospheric heat flux between the two simulations tends to damp rather than to force these anomalies.

5.2. Heat and freshwater transports

Fig. 11 (top panel) displays the ocean heat transport in CM5_piStart across specific sections around the globe. In CM5_piStart, the direction of the heat transport is generally consistent with reconstructions (Greatbatch et al., 1991; Johns et al., 2011) but its intensity is much weaker (0.59 versus 1.2 PW at 30°N). In the North Atlantic, it can be associated to a very weak meridional overturning, as commented by Escudier et al. (2012) that partly explains the strong cold bias described above. In the North Pacific, northward heat transport is also consistent but weaker than in Ganachaud and Wunsch (2000): 0.46 PW in CM5_piStart at 30°N vs. 0.5 PW in the estimates.

0.26 PW of heat enters the Southern Pacific and 1.07 PW are exiting the Indian Ocean towards the Southern Ocean in CM5_piStart. This is again weaker than estimations of Ganachaud and Wunsch (2000) (0.6 PW and 1.5 PW respectively), but consistent in terms of direction. Note that on the contrary, Talley (2003) diagnoses a southward heat transport in the South Pacific (0.39 PW), probably because of a much weaker estimation of the Indonesian Throughflow (ITF). The weak heat exchanges at the northern border of the southern oceans in CM5_piCtrl are consistent with the strong cold anomalies in the southern subpolar area shown in Fig. 8 (top left).

Fig. 11 (lower panel) shows the major differences between CM5_piStart and CM5_RETRO both in terms of heat transport (arrows) and of atmospheric heat flux (colours). Transport (flux) differences that are not significant at the 95% level according to a Student test are not plotted (dotted). If the oceanic drift is small or at least similar in the two simulations, the total budget of the atmospheric flux and divergence of oceanic transport should be comparable. Fig. 1 (top panel) shows that it is indeed the case for the upper 300 m, and it can also be verified for the whole water column (not shown). Thus, in Fig. 11 (and similarly in Fig. 12), changes in oceanic heat transport can be interpreted in terms of changes in atmospheric heat fluxes and conversely. Regarding the heat transport, major differences are found again in the

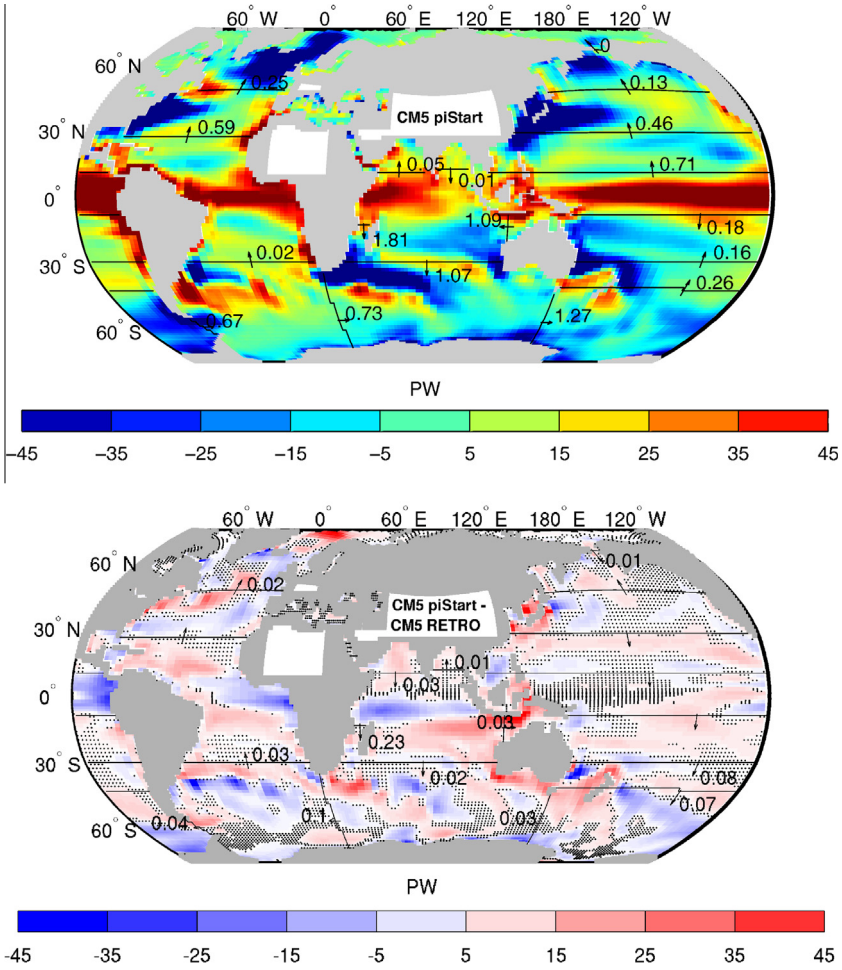

Fig. 11. Colors: total atmospheric heat flux (positive into the ocean) in CM5_piStart (top), and difference between CM5_piStart and CM5_RETRO (bottom). Black arrows: Annual mean transport of heat (PW) by the ocean in CM5_piStart (top) an differences between CM5_piStart and CM5_RETRO (bottom). All averages are computed over the years [2200–2291] of simulations. Black dots on bottom panels show areas where the difference between the two runs is not significant at the 95% level according to a Student test under the assumption that the variance is unchanged. Only the transports differences significant at the same level and according to the same test are indicated.

southern basins. The zonal heat transport in the Southern Ocean is weaker (by 2–10%) in CM5_piStart than in CM5_RETRO. Differences are largest at the longitude of the Cape of Good Hope. At 30°S in the South Atlantic, both the very weak northward transport in CM5_piStart (0.02 PW) and the very weak southward one in CM5_RETRO (0.01 PW) are unrealistic (0.35 PW northward in Ganachaud and Wunsch, 2000; Talley, 2003). Nevertheless, the weaker transport at Cape of Good Hope in CM5_piStart could be explained by a weak northern loss in the southern Atlantic as compared to CM5_RETRO. This effect is however not strong enough to explain the whole difference. Variations of ACC heat transport are also explained by its meanders, as shown by Sun and Watts (2002): the ACC warms when it meanders equatorward, namely in the South Atlantic and Indian Oceans, mainly thanks to the Brazil and Agulhas western boundary currents, and cools in its poleward segments, primarily in the South Pacific. This feature in well reproduced in both simulations. The largest zonal changes in water mass heat content in CM5 RETRO is not associated with a strong change in mass transport (Fig. 13 below) and it could thus be due to stronger temperature gradients in the Brazil-Falkland confluence in this simulation compared to CM5_piStart (not shown).

The northward heat transport entering the South Pacific is also weaker in CM5_piStart than in CM5_RETRO. This is consistent with the stronger oceanic heat uptake from the atmosphere between 15°S and 30°S. Reduced ITF in CM5_piStart compared to CM5_RETRO is also consistent with reduced northward (intensified southward) heat flux into the Arabian Sea. Again, this implies an excess of heat in the Arabian Sea, which is taken from the atmosphere.

In the North Atlantic, the northward heat transport at 30°N is unchanged in the two simulations. The slight intensification (0.02 PW) seen at 45°N is associated with intensified mass and AMOC transport, as discussed below. Furthermore, an intensification of the oceanic heat transport at 45°N is consistent with a capture of heat from the atmosphere into the ocean between 30°N and 45°N, as seen along the North Atlantic Current path (Fig. 11 bottom colours).

Fig. 12 shows the annual mean transport of freshwater (in mSv, using 34.8 psu as a reference) across the same selected sections. This figure can be compared to estimates by Talley et al., 2003) (the net volume transports were removed prior to computing the freshwater transports). The sign of these transports generally agrees with the observations: The ACC transports freshwater eastward, which enters at the southern edge of each oceanic basin. In the North Atlantic and North Pacific, on the other hand, the net transport is southward, and convergences occur in the subtropics, where evaporation (colours) is maximum. Comparing CM5_piStart and CM5_RETRO, we notice generally a qualitative compensation in terms of density between the anomalous heat and freshwater transports, in particular in the Atlantic and the Indian oceans and zonally in the Southern Ocean. In the tropics, anomalies of the total

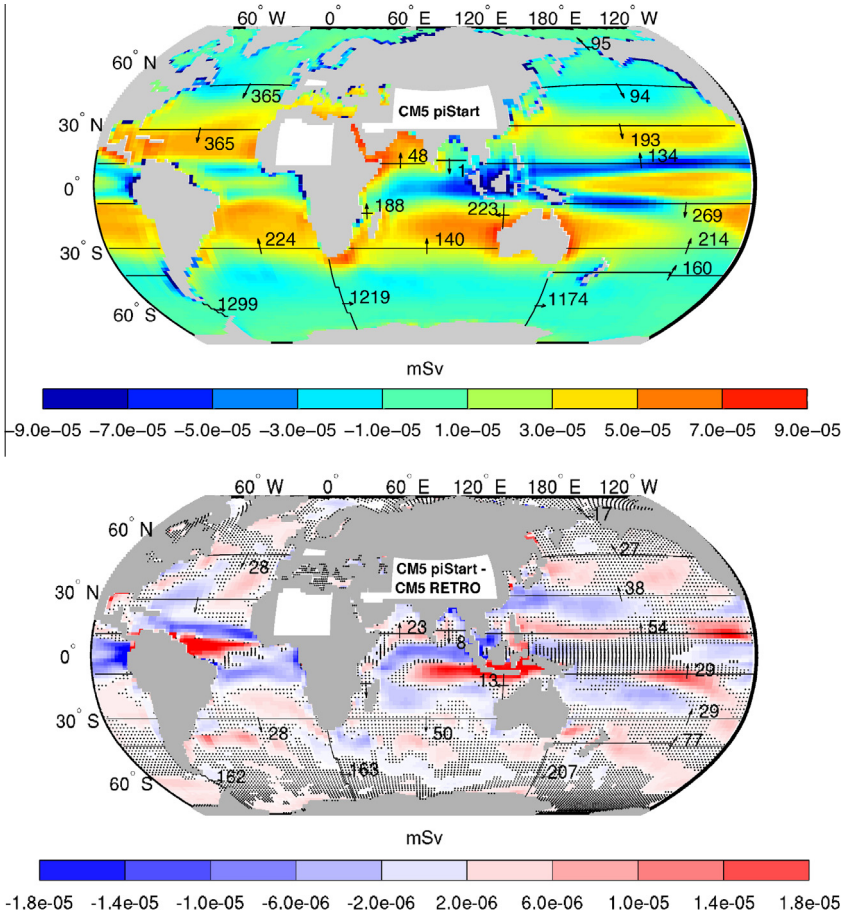

Fig. 12. Colors: total atmospheric freshwater flux (positive out of the ocean) in CM5_piStart (top), and differences between CM5_piStart and CM5_RETRO (bottom). Black arrows: Annual mean transport of freshwater (mSv) by the ocean in CM5_piStart (top) and differences between CM5_piStart and CM5_RETRO (bottom). All averages are computed over the years [2200–2291] of simulations. Black dots on bottom panels show areas where the difference between the two runs is not significant at the 95% level according to a Student test under the assumption that the variance is unchanged. Only the transports differences significant at the same test are indicated.

atmospheric freshwater fluxes out of the ocean are generally strong, except in the Pacific, and consistent with a northward shift of the ITCZ in CM5_piStart in the Atlantic and the Indian Ocean, as described above. In the Pacific, anomalous freshwater fluxes are rather indicative of a stronger SPCZ (or double ITCZ) (not shown). All these changes in the atmospheric flux induce associated salinity anomalies in surface as described earlier (Fig. 4). Finally, as indicated above, strong changes are also found in the northern Indian basin, where colder conditions in CM5_piStart induce less evaporation and weakened northward freshwater.

5.3. Oceanic circulation

Fig. 13 shows the total net mass transport across the same selected sections as for the heat and freshwater transport in CM5_piStart (top) and in terms of differences between CM5_piStart and CM5_RETRO (bottom). The net mass transport is generally stronger in CM5_piStart than in CM5_RETRO. At the Drake Passage, in particular, the total transport amounts about 109 Sv in CM5_piStart, which is 23% more than in CM5_RETRO, but still weaker than the value inferred from observations (136.7 ± 7.8 Sv Cunningham et al., 2003). Such an intensification of the ACC from AR4 to AR5 configuration is very close to the 21% increase diagnosed in the forced configurations described above. This suggests an important role of the changes in the oceanic component in this evolution (rather than changes in the atmosphere, impacting wind stress for instance). The weak ACC intensity was a known deficiency of the IPSL-CM4 climate model (e.g. Marti et al., 2010; Marini et al., 2010). The latter is enhanced from 50 Sv in CM4_piCtrl (references above) to 98 Sv in CM5_piCtrl (Fig. 1), thus an increase of roughly 50%, which is twice as much as what is found from CM5_RETRO to CM5_piStart (Fig. 13). This indicates that the change in atmospheric horizontal resolution also plays an important role, as explained in Hourdin et al. (2012) and also underlined by Marti et al. (2010). Note also that these numbers highlight the fact that CM5_piStart (and thus also probably CM5_RETRO) is not in full equilibrium, as the intensity of the flow through the Drake Passage in this simulation (109 Sv) slightly differs from what is found in CM5-piCtrl (98 Sv). Finally, intensification of the ACC in CM5_piStart is consistent with strengthening of the density gradient across the Southern Ocean, as described above (Fig. 10), but this does not allow distinguishing causality. On the other hand, it contrasts with the weaker eastward heat transport seen in Fig. 11, demonstrating the importance of meridional temperature gradients and meanders for this heat transport (Sun and Watts, 2002).

Downstream of the Drake Passage, the circumpolar transport of mass is fed in both simulations by a weak input from the South Atlantic and a stronger one from the Indian Ocean, consistent with inversions from Ganachaud and Wunsch (2000). In both simulations, it thus slightly increases from the Drake Passage to the Cape of Good Hope and Cape Leewin sections. In the Pacific, the net mass transport is northward at all latitudes. This is again consistent with Ganachaud and Wunsch (2000). Their inversion yields an Indonesian Throughflow of 16 Sv, and the latest long-term simultaneous

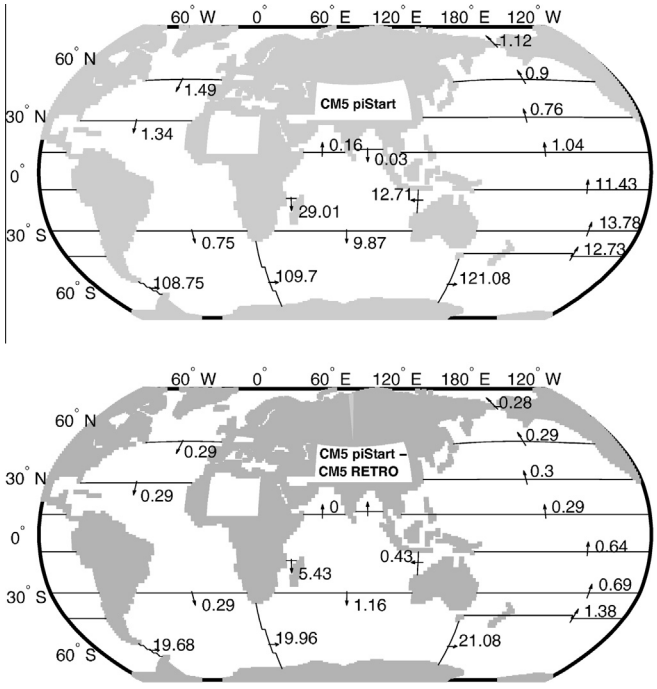

Fig. 13. Annual mean net mass transport for piStart (top) and differences between CM5-piStart and CM5_RETRO (bottom). Averaged over 220–2291. Both the lagrangian and the eddy induced component have been accounted for. Only the transports differences significant at the same level and according to the same test are indicated.

measurements within both inflow and outflow passages (INSTANT 2004–2006) estimated a total transport of 14 ± 3 Sv (Sprintall et al., 2009). The intensity of the Indonesian Throughflow in terms of net mass transport in CM5_piStart is lower than these estimates (12.7 Sv Fig. 13), slightly stronger than in CM5_RETRO (12.3 Sv), although the difference is probably not significant. This might be again a consequence from the implementation of the ITF parameterisation developed by Koch-Larrouy et al. (2009) in CM5_piStart.

Fig. 14 (left panels) compares the global mean meridional circulation for the years [2200–2291] of each simulation. The major difference lies in intensification by roughly 12 Sv of the Antarctic Bottom Water circulation in the Southern Hemisphere in CM5_piStart as compared to CM5_RETRO. This increase is roughly portioned among the oceanic basins according to their width, as this cell increases by 4 Sv at the southern bottom of the Indian Ocean, 5 Sv in the Pacific and only 3 Sv in the Atlantic (not shown). As seen above for the forced simulations, this intensification is consistent with the evolution of the oceanic component, and in particular the implementation of the *kz-tide* parameterization. It is associated with notable temperature and more importantly salinity modifications in the Southern Ocean and along the sea floor, as described above.

The shallow subtropical cells are very similar in the two simulations, consistent with comparable mean wind stress field and wind stress curl (not shown). Regarding the upper cell of interhemispheric transport, the weak intensification of the global cell (Fig. 14, left panels) is due to the North Atlantic contribution (Fig. 14 right panels). At 26°N, the intensity of the overturning component of mass transport is much weaker both in CM5_RETRO (7.3 Sv) and in CM5_piStart (8.7 Sv) than what is suggested by observations (e.g. 18.7 ± 5.6 Sv Cunningham et al., 2007). At this location, intensification from CM5_RETRO to CM5_piStart configuration amounts to 15%, and this value is similar for all subtropical latitudes. Further north, differences are smaller (8.0 Sv in CM5_RETRO vs 8.4 Sv in CM5_piStart. at 45°N) and values are again weaker than values inferred from observations (14–15 Sv in Ganachaud and Wunsch, 2000; Talley et al., 2003), as already commented in several studies (Dufresne et al., 2013; Marti et al., 2010; Swingedouw et al., 2007).

Finally, the barotropic streamfunction (Fig. 15) confirms that the Antarctic Circumpolar Current (ACC) is stronger in CM5_piStart than in CM5_RETRO after 400 years of simulation. Beyond the Southern Ocean, major changes are found in the Pacific, with a basin-wide positive anomaly in CM5_piStart in the northern mid-latitudes and a negative one in the south. Given the lack of significant differences in the wind stress curl structure and intensity in both simulations (not shown), these differences could be due to changes in the oceanic bathymetry. The black lines in Fig. 15 (bottom panel) indeed show that several areas, including the North Pacific, are much deeper in CM5_piStart than in CM5_RETRO. This modification was implemented simultaneously as the partial steps formulation: the last level of the model in abyssal plains was increased in CM5_piStart to improve realism of the topography. This deeper bathymetry in CM5_piStart induces a decrease of the potential vorticity expressed as f/H where f stands for the Coriolis factor and H the local depth of the ocean. This is consistent with the generally positive anomalies in the barotropic streamfunction in the northern Pacific in CM5_piStart and the negative ones in the south (Fig. 15 bottom panel). In the North Pacific, the intensity of both gyres (maximum of the streamfunction of the each gyre) is nevertheless weaker in CM5_piStart (55 Sv vs. 59 Sv in CM5_RETRO for the subtropical gyre, 21 Sv vs. 27 Sv in CM5_RETRO for the subpolar gyre).

The change from one model to the next is similar but smaller in the other basins, except for the North Atlantic, where the subpolar gyre is intensified (18 Sv in CM5_piStart, vs. 16 Sv in CM5_RETRO) in CM5_piStart in spite of small changes in bathymetry. This intensification is due to the intensification of the deep convection in this area (not shown) that compensates a decrease of deep convection in the Nordic Seas linked to the increase of sea-ice extent. Observations-based estimates are nevertheless around 40 Sv for the subpolar gyre (Hakkinen and Rhines, 2004), so that the circulation remains very weak in CM5_piStart, consistently with the weak AMOC described above and as was the case in CM5_piCtrl (Escudier et al., 2012) and CM4_piCtrl (Marti et al., 2010). The intensity of the North Atlantic subtropical gyre is around 40 Sv in both CM5_RETRO and CM5_piStart, and 60 Sv in observations-based estimates (Greatbatch et al., 1991,Johns et al.; 1995).

6. Conclusions

This paper describes the evolution of the oceanic component of the climate model developed at Institut Pierre Simon Laplce (IPSL) from the version IPSL-CM4, used for CMIP3, to IPSL-CM5A, contributing to the ongoing CMIP5. Several modifications have been implemented between these two versions, in particular the inclusion of an interactive coupling with a biogeochemical module, a 3-band model for the penetration of the solar radiation, partial steps at the bottom of the ocean and a series of dynamical parameterisations to improve the representation of the Langmuir cells and of the tidal mixing. A set of forced and coupled experiments was used here to analyse as accurately as possible the effect of each of these modifications and more generally the evolution of the oceanic component of the IPSL coupled models family. Although all necessary sensitivity experiments were not available to properly disentangle the respective effect of each modification, we believe that it is important to illustrate and explain how the ocean model changes have modified the mean oceanic circulation and thermohaline properties in the framework of CMIP5 where different groups will intensively use this coupled model worldwide. In terms

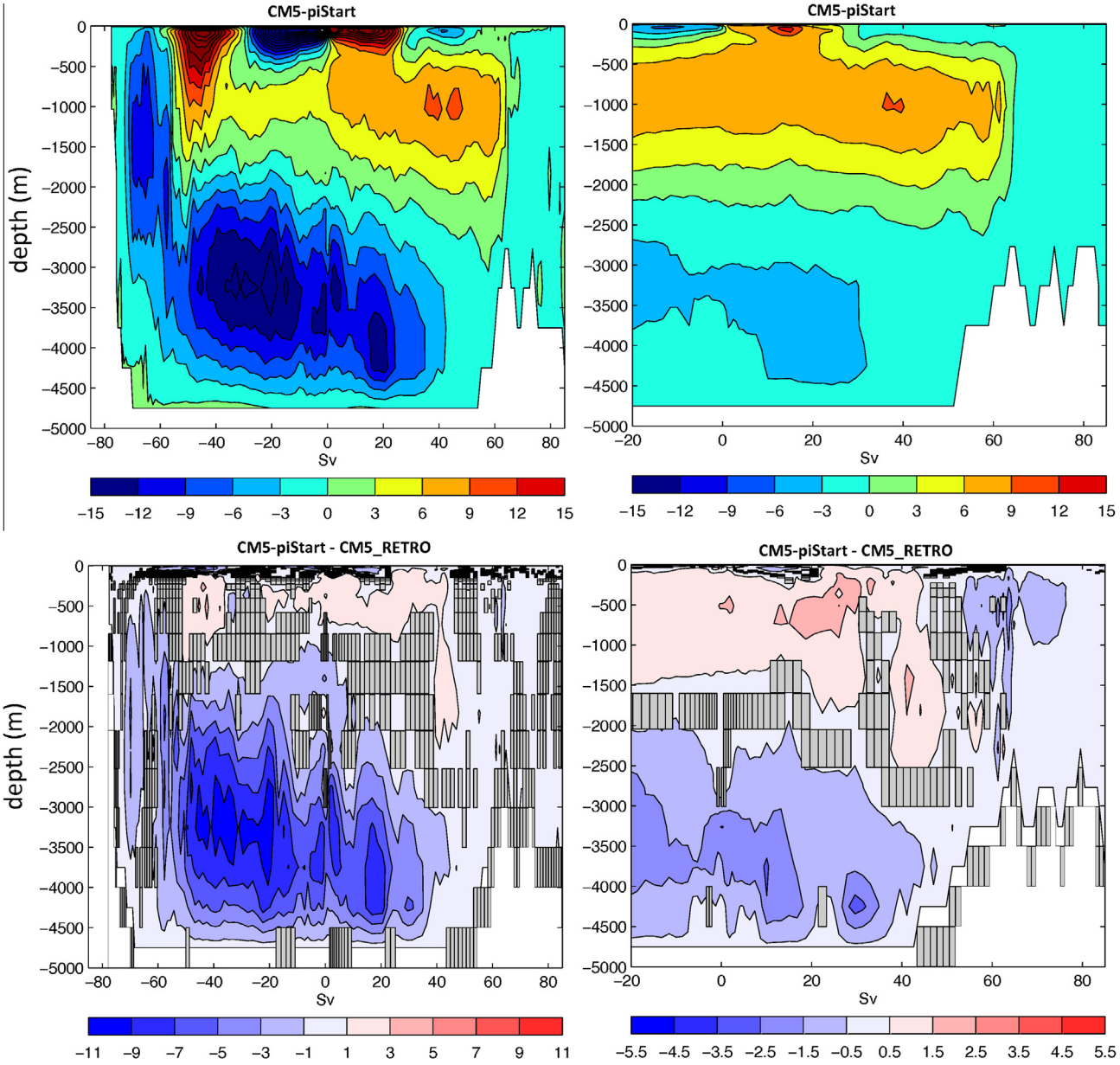

Fig. 14. Global (left panels) and Atlantic (right panels) meridional streamfunction averaged over years 2200–2291 in CM5_piStart (top) and differences between CM5_piStart and CM5_RETRO (bottom). Grey shading on bottom panels show areas where the difference between the two runs is not significant at the 95% level according to a Student test under the assumption that the variance is unchanged.

of climate modelling, this study demonstrates the difficulty to tune a coupled model, given the variety of parameters and the compensating effects. In terms of ocean modelling more specifically, this study was a good opportunity to underline the effect of specific parameterizations in forced and coupled mode respectively, as well as interactions with biogeochemistry.

Analysis of forced simulations reveals that modifications of the bathymetry and parameterisation of tidal-driven mixing had a major effect on the dynamics, especially in the Southern Hemisphere. Implementation of partial steps primarily strengthens the Antarctic Circumpolar Current mass transport while tidal mixing strongly impacts water masses flow within the Indonesian Archipelago as well as the representation of Antarctic Bottom waters formation and circulation. Properties of this water mass are also more realistic.

The effect of including an interactive biogeochemistry was investigated in coupled mode, using twin experiments designed purposely. During the first decade of the simulation, this effect broadly agrees with results from previous studies, inducing a surface warming and subsurface cooling in eutrophic regions and the opposite in oligotrophic regions. Within the mid to high latitude oceans, the interactive biogeochemical module also induces an intensification of the seasonal cycle of the sea surface temperature in agreement with the literature. However, during the following decades, the surface cooling progressively intensifies in our simulation to largely overwhelm the summer local warming, thus imprinting the annual mean response on the long term. The inclusion of the biogeochemical component thus generally acts to cool the upper ocean up to 300 m depth. This response is rather large and dominates the hydrographical differences between CM4_piCtrl and CM5_piCtrl. This is due to the specific profile of the chlorophyll in IPSL-CM5A, which translates substantial differences in nutrient distribution, incoming shortwave or ocean circulation as compared to IPSL-CM4. However, further work is needed to single out what prominent drivers are behind this change in the vertical profile of chlorophyll.

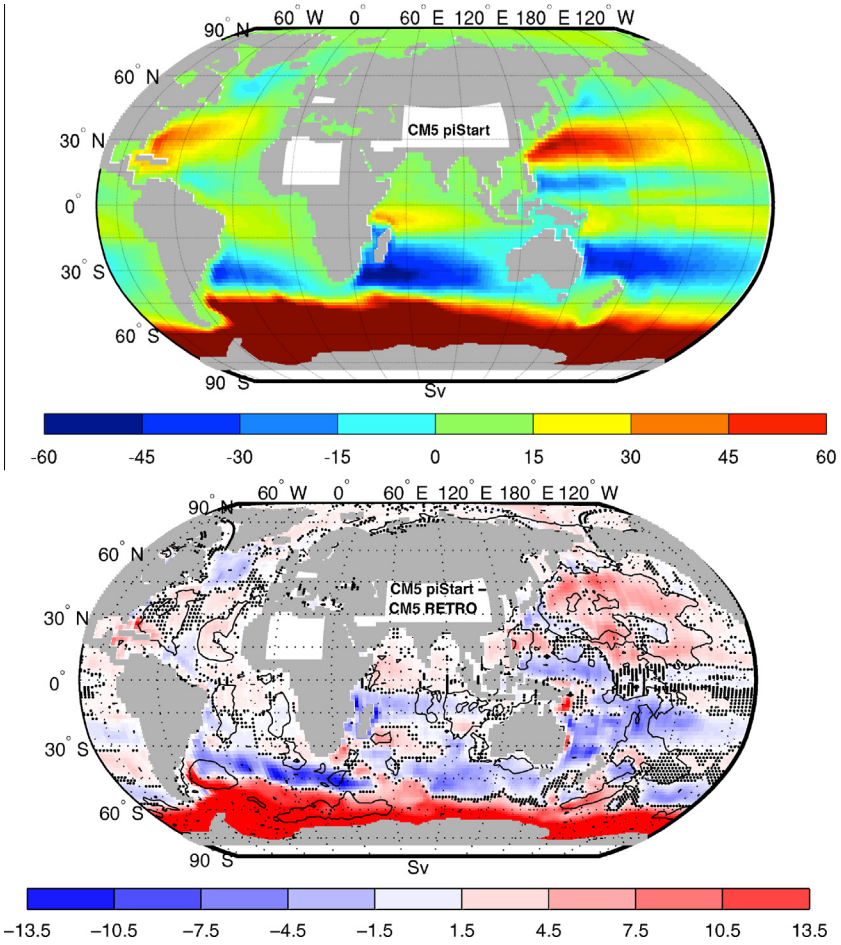

Fig. 15. Top: baratropic stremafunction in CM5_piStart. Bottom: in CM5_RETRO as compared to CM5_piStart. The black contours highlight regions where the bathymetry has changed by more than 800m between the two version because of abyssal plains. Solid lines show areas where the bathymetry is deeper in CM5_RETRO. All averages are computed over the years [2200–2291] of simulations. Black dots on bottom panels show areas where the difference between the two runs is not significant at the 95% level according to a Student test under the assumption that the variance is unchanged.

Finally, two simulations integrated in parallel using rigorously the same atmospheric component and ocean initial conditions but oceanic models corresponding to the control version IPSL-CM5A and IPSL-CM4 respectively (thus differing by all aspects discussed above), named CM5_piStart and CM5_RETRO, were analysed. The sign of surface temperature anomalies between CM5_piStart and CM5_RETRO is consistent with the effects of the biological module. Nevertheless, the amplitude of the differences in SST between CM5_piStart and CM5_RETRO are much larger than between CM5_piCtrl and CM5_piCtrl_noBio. Dynamical adjustments induced by additional parameterisations in the oceanic model indeed led to major improvements in particular in the representation of the Southern Ocean both thermodynamically (meridional density gradient) and dynamically (water mass transport). In particular, these changes have enabled a strengthening of the barotropic flow of water mass of the Antarctic circumpolar current by about 20% and of the northward flow of Antarctic bottom water by about 17%. Below the surface, the amplitude of the differences between CM5_piCtrl and CM5_piCtrl_noBio is similar to the differences between CM5_piStart and CM5_RETRO, suggesting a leading role of the interactive biogeochemical module.

Despite a stronger mass transport, the zonal ocean heat transport in the Southern Ocean is even more underestimated in CM5_piStart than in CM5_RETRO as compared to a global inverse model based on observations (0.8 PW in Talley, 2003). This could partly come from an unrealistic southward heat transport in the South Atlantic in the former version, as well as from the thermal structure in the Southern Ocean. Indeed, most improvements in this region described above were shown to be dominated by salinity. In general, both heat and freshwater transport changes were found to be consistent with atmospheric fluxes and dynamic adjustments, and helpful in interpreting the latter.

In terms of ocean modelling, some issues remain to be explored: the TKE scheme proposed in F4 for example was not kept for the final coupled version because of its negative effect on the seasonal cycle of the SST and in spite of improvements on the temperature climatology. Further work and additional sensitivity experiments should help clarify this point.

Acknowledgments

Analysis of heat, freshwater and volume transport was done using PAGO (http://www.whoi.edu/science/PO/pago/). DS thanks Laurent Bopp and Christian Ethé for their help in the setup of the CM5_piCtrl_NoBio simulation. Arnaud Caubel, Sébastien Denvil, Marie-Alice Foujols and the whole team of the "pole de modélisation de l'IPSL" are also acknowledged for their work in carrying CMIP3 and 5 simulations from IPSL. This work has benefited from the support of LEFE-MISSTERRE. The authors are grateful to the reviewers and editor for their valuable comments which helped to improve the manuscript.

References

Aumont, O., Bopp, L., 2006. Globalizing results from ocean in situ iron fertilization studies. Global Biogeochem. Cycles 20. http://dx.doi.org/10.1029/2005GB002591.

Aumont, O., Maier-Reimer, E., Blain, S., Monfray, P., 2003. An ecosystem model of the global ocean including Fe, Si, P colimitations. Global Biogeochem. Cycles 17 (2). http://dx.doi.org/10.1029/2001GB001745.

Axell, L.B., 2002. Wind-driven internal waves and Langmuir circulations in a numerical ocean model of the southern Baltic Sea. J. Geophys. Res. 107 (C11). http://dx.doi.org/10.1029/2001JC000922.

Barnier, B., Madec, G., Penduff, T., Molines, J.-M., Treguier, A.-M., Sommer, J., Beckmann, A., Biastoch, A., Böning, C., Dengg, J., Derval, C., et al., 2006. Impact of partial steps and momentum advection schemes in a global ocean circulation model at eddy-permitting resolution. Ocean Dyn. 56, 543–567. http://dx.doi.org/10.1007/s10236-006-0082-1.

Bellenger, H., Guilyardi, E., Leloup, J., Lengaigne, M., Vialard, J., 2013. ENSO representation in climate models: from CMIP3 to CMIP5. Clim. Dyn. http://dx.doi.org/10.1007/s00382-013-1783-z.

Blanke, B., Delecluse, P., 1993. Variability of the tropical Atlantic Ocean simulated by a general circulation model with two different mixed-layer physics. J. Phys. Oceanogr. 23, 1363–1388.

Born, A., Mignot, J., 2011. Dynamics of decadal variability in the Atlantic subpolar gyre: a stochastically forced oscillator. Clim. Dyn. 39 (1–2), 461–474. http://dx.doi.org/10.1007/s00382-011-1180-4.

Braconnot, P., Marti, O., Joussaume, S., 1997. Adjustment and feedbacks in a global coupled ocean-atmosphere model. Clim. Dyn. 13 (7–8), 507–519. http://dx.doi.org/10.1007/s003820050179.

Brix, H., Gerdes, R., 2003. North Atlantic deep water and Antarctic bottom water: their interaction and influence on the variability of the global ocean circulation. J. Geophys. Res. 108 (C2), 78–96. http://dx.doi.org/10.1029/2002JC001335.

Burchard, H., 2002. Energy-conserving discretisation of turbulent shear and buoyancy production. Ocean Model. 4, 347–361. http://dx.doi.org/10.1016/S1463-5003(02)00009-4.

Carrère, L., Lyard, F., 2003. Modeling the barotropic response of the global ocean to atmospheric wind and pressure forcing – comparisons with observations. Geophys. Res. Lett. 30 (6). http://dx.doi.org/10.1029/2002GL016473.

Clarke, P.U., Pisias, N.G., Stocker, T.F., Weaver, A.J., 2002. The role of the thermohaline circulation in abrupt climate change. Nature 415, 863–869.

Conkright, M.E., Boyer, T.P., 2001. World Ocean Atlas 2001: Objective Analyses, Data Statistics, and Figures.

Cunningham, A.S., Kanzow, T., Rayner, D., Baringer, M.O., Johns, W.E., Marotzke, Longworth, H.R., Grant, E.M., Hirschi, J.J.-M., Beal, L.M., Meinen, C.S., 2007. Temporal variability of the atlantic meridional overturning circulation at 26.5 °N. Science 317, 935–938. http://dx.doi.org/10.1126/science.1141304.

Cunningham, S.A., Alderson, S.G., King, B.A., Brandon, M.A., 2003. Transport and variability of the antarctic circumpolar current in drake passage. J. Geophys. Res. 108 (C5), 8084. http://dx.doi.org/10.1029/2001JC001147.

Davey, M., Huddleston, M., Sperber, M., Braconnot, P., Bryan, F., Chen, D., Colman, R., Cooper, C., Cubasch, U., Delecluse, P., DeWitt, B., et al., 2002. STOIC: a study of coupled model climatology and variability in tropical ocean regions. Clim. Dyn. 18 (5), 403–420. http://dx.doi.org/10.1007/s00382-001-0188-6.

Delworth, T.L., Mann, M.E., 2000. Observed and simulated multidecadal variability in the northern hemisphere. Clim. Dyn. 16 (9), 661–676. http://dx.doi.org/10.1007/s003820000075.

Dijkstra, H.A., Raa, L., Schmeits, M., Gerrits, J., 2006. On the physics of the Atlantic multidecadal oscillation. Ocean Dyn. 56 (1), 36–50. http://dx.doi.org/10.1007/s10236-005-0043-0.

Downes, S.M., Gnanadesikan, A., Griffies, S.M., Sarmiento, J.L., 2011. Water mass exchange in the southern ocean in coupled climate models. J. Phys. Oceanogr. 41 (9), 1756–1771. http://dx.doi.org/10.1175/2011JPO4586.1.

Dufresne, J.-L., Foujols, M.-A., Denvil, S., Caubel, A., Marti, O., Aumont, O., Balkanski, Y., Bekki, S., Bellenger, H., Benshila, R., Bony, S., et al., 2013. Climate change projections using the IPSL-CM5 earth system model: from CMIP3 to CMIP5. Clim. Dyn. http://dx.doi.org/10.1007/s00382-012-1636-1.

Duteil, O., Koeve, W., Oschlies, A., Aumont, O., Bianchi, D., Bopp, L., Galbraith, E., Matear, R., Moore, J.K., Sarmiento, J.L., Segschneider, J., 2011. Preformed and regenerated phosphate in ocean general circulation models: can right total concentrations be wrong? Biogeosci. Discuss. 8 (6), 12423–12449. http://dx.doi.org/10.5194/bgd-8-12423-2011.

Eden, C., Willebrand, J., 2001. Mechanism of interannual to decadal variability of the north Atlantic circulation. J. Climate 14, 2266–2280. http://dx.doi.org/10.1175/1520-0442(2001) 014<2266:MOITDV>2.0.CO;2.

Escudier, R., Mignot, J., Swingedouw, D., 2012. A 20-year coupled ocean-sea ice-atmosphere variability mode in the North Atlantic in an AOGCM. Clim. Dyn. http://dx.doi.org/10.1007/s00382-012-1402-4.

Ganachaud, A., Wunsch, C., 2000. Improved estimates of global ocean circulation, heat transport and mixing from hydrographic data. Nature 408, 453–456.

Gastineau, G., D'Andrea, F., Frankignoul, C., 2012. Atmospheric response to the North Atlantic Ocean variability on seasonal to decadal time scales. Clim. Dyn. 40 (9–10), 2311–2330. http://dx.doi.org/10.1007/s00382-012-1333-0, 2012.

Gastineau, G., Frankignoul, C., 2011. Cold-season atmospheric response to the natural variability of the Atlantic meridional overturning circulation. Clim. Dyn. 39 (1–2), 37–57. http://dx.doi.org/10.1007/s00382-011-1109-y.

Gent, P.R., McWilliams, J.C., 1990. Isopycnal mixing in ocean circulation models. J. Phys. Oceanogr. 20, 150–151.

Gnanadesikan, A., Anderson, W.G., 2009. Ocean water clarity and the ocean general circulation in a coupled climate model. J. Phys. Oceanogr. 39 (2), 314–332. http://dx.doi.org/10.1175/2008JPO3935.1.

Greatbatch, R.J., Fanning, A.F., Goulding, A.D., Levitus, S., 1991. A diagnosis of interpentadal circulation changes in the north Atlantic. J. Geophys. Res. 96 (C12), 22009–22023. http://dx.doi.org/10.1029/91JC02423.

Griffies, S.M., Biastoch, A., Böning, C., Bryan, F., Danabasoglu, G., Chassignet, E.P., England, M.H., Gerdes, R., Haak, H., Hallberg, R.W., Hazeleger, W., et al., 2009. Coordinated ocean-ice reference experiments (COREs). Ocean Model. 26, 1–46. http://dx.doi.org/10.1016/j.ocemod.2008.08.007.

Guemas, V., Codron, F., 2011. Differing impacts of resolution changes in latitude and longitude on the mid-latitudes in the LMDZ Atmospheric GCM. J. Clim. 24 (22), 5831–5849. http://dx.doi.org/10.1175/2011JCLI4093.1.

Hakkinen, S., Rhines, P.B., 2004. Surface salinity variability in the northern North Atlantic during recent decades. Science 304 (5670), 555–559. http://dx.doi.org/10.1126/science.1094917.

Hourdin, F., Foujols, M.-A., Codron, F., Guemas, V., Dufresne, J.-L., Bony, S., Denvil, S., Guez, L., Lott, F., Ghattas, J., Braconnot, P., et al., 2012. Impact of the LMDZ atmospheric grid configuration on the climate and sensitivity of the IPSL-CM5A coupled model. Clim. Dyn. http://dx.doi.org/10.1007/s00382-012-1411-3.

Hourdin, F., Musat, I., Bony, S., Braconnot, P., Codron, F., Dufresne, J.-L., Fairhead, L., Filiberti, M.-A., Friedlingstein, P., Grandpeix, J.-Y., Krinner, G., et al., 2006. The LMDZ4 general circulation model: climate performance and sensitivity to parametrized physics with emphasis on tropical convection. Clim. Dyn. 27 (7–8), 787–813. http://dx.doi.org/10.1007/s00382-006-0158-0.

Huang, B., Schneider, E.K., 1995. The response of an ocean general circulation model to surface wind stress produced by an atmospheric general circulation model. Mon. Weather Rev. 123 (10), 3059–3085. http://dx.doi.org/10.1175/1520-0493(1995) 123<3059:TROAOG>2.0.CO;2.

Jacket, D.R., McDougall, T.J., 1995. Minimal adjustment of hydrographic data to achieve static stability. J. Atmos. Ocean. Technol. 12, 381–389.

Jerlov, N.G., 1968. Optical Oceanography. Elsevier.

Johns, W.E., Baringer, M.O., Beal, L.M., Cunningham, S.A., Kanzow, T., Bryden, H.L., Hirschi, J.J.M., Marotzke, J., Meinen, C.S., Shaw, B., Curry, R., 2011. Continuous, array-based estimates of Atlantic Ocean heat transport at 26.5°N. Journal of Climate 24 (10), 2429–2449. http://dx.doi.org/10.1175/2010JCLI3997.1.

Johns, W.E., Shay, T.J., Bane, J.M., Watts, D.R., 1995. Gulf Stream structure, transport, and recirculation near 68°W. J. Geophys. Res. 100 (1), 817–838. http://dx.doi.org/10.1029/94JC02497.

Kerr, R.A., 2000. A north Atlantic climate pacemaker for the centuries. Science 288 (5473), 1984–1985. http://dx.doi.org/10.1126/science.288.5473.1984.

Kiehl, J.T., Gent, P.R., 2004. The community climate system model, version 2. J. Clim. 17 (19), 3666–3682. http://dx.doi.org/10.1175/1520-0442(2004)017<3666:TCCSMV>2.0.CO;2.

Koch-Larrouy, A., Lengaigne, M., Terray, P., Madec, G., Masson, S., 2009. Tidal mixing in the Indonesian Seas and its effect on the tropical climate system. Clim. Dyn. 34 (6), 891–904. http://dx.doi.org/10.1007/s00382-009-0642-4.

Koch-Larrouy, A., Madec, G., Blanke, B., Molcard, R., 2008a. Water mass transformation along the Indonesian throughflow in an OGCM. Ocean Dyn. 58, 289–309. http://dx.doi.org/10.1007/s10236-008-0155-4.

Koch-Larrouy, A., Madec, G., Bouruet-Aubertot, P., Gerkema, T., Bessières, L., Molcard, R., 2007. On the transformation of Pacific water into Indonesian throughflow water by internal tidal mixing. Geophys. Res. Lett. 34 (4). http://dx.doi.org/10.1029/2006GL028405.

Koch-Larrouy, A., Madec, G., Iudicone, D., Atmadipoera, A., Molcard, R., 2008b. Physical processes contributing to the water mass transformation of the Indonesian throughflow. Ocean Dyn. 58, 275–288. http://dx.doi.org/10.1007/s10236-008-0154-5.

Krinner, G., Viovy, N., de Noblet-Ducoudré, N., Ogée, J., Polcher, J., Friedlingstein, P., Ciais, P., Sitch, S., Prentice, I.C., 2005. A dynamic global vegetation model for studies of the coupled atmosphere-biosphere system. Glob. Biogeochem. Cycles 19 (1). http://dx.doi.org/10.1029/2003GB002199.

Lefebvre, V., Donnadieu, Y., Sepulchre, P., Swingedouw, D., Zhang, Z.-S., 2012. Deciphering the role of southern gateways and carbon dioxide on the onset of the Antarctic circumpolar current. Paleoceanography 27 (4). http://dx.doi.org/10.1029/2012PA002345.

Lefèvre, F., Brasseur, G.P., Folkins, I., Smith, A.K., Simon, P., 1994. Chemistry of the 1991–1992 stratospheric winter: three-dimensional model simulations. J. Geophys. Res. 99 (D4), 8183. http://dx.doi.org/10.1029/93JD03476.

Lefèvre, F., Figarol, F., Carslaw, K.S., Peter, T., 1998. The 1997 Arctic Ozone depletion quantified from three-dimensional model simulations. Geophys. Res. Lett. 25 (13), 2425–2428. http://dx.doi.org/10.1029/98GL51812.

Lengaigne, M., Madec, G., Bopp, L., Menkes, C., Aumont, O., Cadule, P., 2009. Bio-physical feedbacks in the Arctic Ocean using an earth system model. Geophys. Res. Lett. 36. http://dx.doi.org/10.1029/2009GL040145.

Lengaigne, M., Menkes, C., Aumont, O., Gorgues, T., Bopp, L., André, J.-M., Madec, G., 2006. Influence of the oceanic biology on the tropical Pacific climate in a coupled general circulation model. Clim. Dyn. 28, 503–516. http://dx.doi.org/10.1007/s00382-006-0200-2.

Levermann, A., Born, A., 2007. Bistability of the Atlantic subpolar gyre in a coarse resolution climate model. Geophys. Res. Lett. 34, L24605.

Levitus, S., Boyer, T., 1994. World Ocean Atlas, Volume 4: Temperature, NOAA Atlas NESDIS 4, Washington DC.

Madec, G., 2008. NEMO ocean engine, NEMO ocean engine, Institut Pierre-Simon Laplace, France.
Madec, G., Delecluse, P., Imbart, M., Levy, C., 1999. OPA8.1 Ocean General Circulation Model reference manual, Institut Pierre-Simon Laplace (IPSL), France.
Manizza, M., 2005. Bio-optical feedbacks among phytoplankton, upper ocean physics and sea-ice in a global model. Geophys. Res. Lett. 32 (5). http://dx.doi.org/10.1029/2004GL020778.
Marini, C., Frankignoul, C., 2013. An attempt to deconstruct the Atlantic multidecadal oscillation. Clim. Dyn. http://dx.doi.org/10.1007/s00382-013-1852-3.
Marini, C., Frankignoul, C., Mignot, J., 2010. Links between the Southern annular mode and the Atlantic meridional overturning circulation in a climate model. J. Clim. 24 (3), 624–640. http://dx.doi.org/10.1175/2010JCLI3576.1.
Marsaleix, P., Auclair, F., Floor, J.W., Herrmann, M.J., Estournel, C., Pairaud, I., Ulses, C., 2008. Energy conservation issues in sigma-coordinate free-surface ocean models. Ocean Model. 20, 61–89. http://dx.doi.org/10.1016/j.ocemod.2007.07.005.
Marti, O., Braconnot, P., Dufresne, J.-L., Bellier, J., Benshila, R., Bony, S., Brockmann, P., Cadule, P., Caubel, A., Codron, F., Noblet, N., et al., 2010. Key features of the IPSL ocean atmosphere model and its sensitivity to atmospheric resolution. Clim. Dyn. 34, 1–26. http://dx.doi.org/10.1007/s00382-009-0640-6.
Marzeion, B., Timmermann, A., Murtugudde, R., Jin, F.-F., 2005. Biophysical Feedbacks in the Tropical Pacific. J. Clim. 18 (1), 58–70. http://dx.doi.org/10.1175/JCLI3261.1.
Meehl, G.A., Covey, C., McAvaney, B., Latif, M., Stouffer, R.J., 2005. Overview of the coupled model intercomparison project. Bull. Am. Meteor. Soc. 86 (1), 89–93. http://dx.doi.org/10.1175/BAMS-86-1-89.
Mellor, G., Blumberg, A., 2004. Wave breaking and ocean surface layer thermal response. J. Phys. Oceanogr. 34, 693–698. http://dx.doi.org/10.1175/2517.1.
Mellor, G., Mechoso, C., Keto, E., 1982. A diagnostic calculation of the general circulation of the Atlantic Ocean. Deep-Sea Res. 29, 1171–1192.
Mikolajewicz, U., Voss, R., 2000. The role of the individual air-sea flux components in CO 2 -induced changes of the ocean's circulation and climate. Clim. Dyn. 16 (8), 627–642. http://dx.doi.org/10.1007/s003820000066.
Morel, A., 1988. Optical modeling of the upper ocean in relation to its biogenous matter content (case I waters). Journal of Geophysical Research 93 (C9), 10749. http://dx.doi.org/10.1029/JC093iC09p10749.
Msadek, R., Frankignoul, C., 2008. Atlantic multidecadal oceanic variability and its influence on the atmosphere in a climate model. Clim. Dyn. 33 (1), 45–62. http://dx.doi.org/10.1007/s00382-008-0452-0.
Myers, P.G., 2002. SPOM: A regional model of the sub-polar north Atlantic. Atmos. Ocean 40 (4), 445–463. http://dx.doi.org/10.3137/ao.400405.
Nikulin, G., Lott, F., 2010. On the time-scales of the downward propagation and of the tropospheric planetary wave response to the stratospheric circulation. Ann. Geophys. 28 (2), 339–351. http://dx.doi.org/10.5194/angeo-28-339-2010.
Pacanowski, R.C., Gnanadesikan, A., 1998. Transient response in a z-level ocean model that resolves topography with partial cells. Mon. Weather Rev., 3248–3270.
Patara, L., Vichi, M., Masina, S., Fogli, P.G., Manzini, E., 2012. Global response to solar radiation absorbed by phytoplankton in a coupled climate model. Clim. Dyn. 39 (7–8), 1951–1968. http://dx.doi.org/10.1007/s00382-012-1300-9.
Paulson, C.A., Simpson, J.J., 1977. Irradiance measurements in the upper ocean. J. Phys. Oceanogr. 7, 952–956.
Penduff, T., Le Sommer, J., Barnier, B., Treguier, A.-M., Molines, J.-M., Madec, G., 2007. Influence of numerical schemes on current-topography interactions in 1/4 degrees global ocean simulations. Ocean Science 3 (4), 509–524.
Penven, P., 2005. Average circulation, seasonal cycle, and mesoscale dynamics of the Peru current system: a modeling approach. J. Geophys. Res. 110 (C10). http://dx.doi.org/10.1029/2005JC002945.
Persechino, A., Mignot, J., Swingedouw, D., Labetoulle, S., Guilyardi, E., 2012. Decadal predictability of the Atlantic meridional overturning circulation and climate in the IPSL-CM5A-LR model. Clim. Dyn. 40 (9–10), 2359–2380. http://dx.doi.org/10.1007/s00382-012-1466-1.
Rahmstorf, S., 2002. Ocean circulation and climate during the past 120,000 years. Nature 419, 207–214.
Roullet, G., Madec, G., 2000. Salt conservation, free surface and varying volume: a new formulation for ocean GCMs. J. Geophys. Res. 105, 23927–23942.
Séférian, R., Bopp, L., Gehlen, M., Orr, J.C., Ethé, C., Cadule, P., Aumont, O., Salas y Mélia, D., Voldoire, A., Madec, G., 2012. Skill assessment of three earth system models with common marine biogeochemistry. Clim. Dyn. http://dx.doi.org/10.1007/s00382-012-1362-8.
Simmons, H., 2004. Tidally driven mixing in a numerical model of the ocean general circulation. Ocean Model. 6, 245–263. http://dx.doi.org/10.1016/S1463-5003(03)00011-8.
Smith, W., Sandwell, D.T., 1997. Global sea-floor topography from satellite altimetry and ship depth souding. Science 277, 1952–1956.
Le Sommer, J., Penduff, T., Theetten, S., Madec, G., Barnier, B., 2009. How momentum advection schemes influence current-topography interactions at eddy permitting resolution. Ocean Model. 29, 1–14. http://dx.doi.org/10.1016/j.ocemod.2008.11.007.
Sprintall, J., Wijffels, S.E., Molcard, R., Jaya, I., 2009. Direct estimates of the Indonesian Throughflow entering the Indian Ocean: 2004–2006. J. Geophys. Res. 114 (C7). http://dx.doi.org/10.1029/2008JC005257.
Sun, C., Watts, D.R., 2002. Heat flux carried by the Antarctic circumpolar current mean flow. J. Geophys. Res. 107 (C9). http://dx.doi.org/10.1029/2001JC001187.
Sweeney, C., Gnanadesikan, A., Griffies, S.M., Harrison, M.J., Rosati, A.J., Samuels, B.L., 2005. Impacts of shortwave penetration depth on large-scale ocean circulation and heat transport. J. Phys. Oceanogr. 35 (6), 1103–1119. http://dx.doi.org/10.1175/JPO2740.1.
Swingedouw, D., Braconnot, P., Delecluse, P., Guilyardi, E., Marti, O., 2007. Impact of global freshwater forcing on the thermohaline circulation: adjustment of the North Atlantic convection sites in a CGCM. Clim. Dyn. 28, 291–305.
Swingedouw, D., Fichefet, T., Huybrechts, P., Goosse, H., Driesschaert, E., Loutre, M.-F., 2008. Antarctic ice-sheet melting provides negative feedbacks on future climate warming. Geophys. Res. Lett. 35 (17). http://dx.doi.org/10.1029/2008GL034410.
Swingedouw, D., Mignot, J., Labetoulle, S., Guilyardi, E., Madec, G., 2012. Initialisation and predictability of the AMOC over the last 50 years in a climate model. Clim. Dyn. 40 (9–10), 2381–2399. http://dx.doi.org/10.1007/s00382-012-1516-8.
Szopa, S., Balkanski, Y., Schulz, M., Bekki, S., Cugnet, D., Fortems-Cheiney, A., Turquety, S., Cozic, A., Déandreis, C., Hauglustaine, D., Idelkadi, A., 2012. Aerosol and ozone changes as forcing for climate evolution between, 1850 and 2100. Clim. Dyn.. http://dx.doi.org/10.1007/s00382-012-1408-y, 2012.
Talley, L.D., 2003. Shallow, intermediate, and deep overturning components of the global heat budget. J. Phys. Oceanogr. 33 (3), 530–560.
Talley, L.D., Reid, J.L., Robbins, P.E., 2003. Data-based meridional overturning streamfunctions for the global oceans. J. Clim. 16, 3213–3226.
Timmermann, R., Goosse, H., Madec, G., Fichefet, T., Ethe, C., Dulière, V., 2005. On the representation of high latitude processes in the ORCA-LIM global coupled sea ice–ocean model. Ocean Model. 8 (1–2), 175–201. http://dx.doi.org/10.1016/j.ocemod.2003.12.009.
Treguier, A.M., Held, I.M., Larichev, V.D., 1997. Parameterization of quasigeostrophic eddies in primitive equation ocean models. J. Phys. Oceanogr. 27 (4), 567–580. http://dx.doi.org/10.1175/1520-0485(1997) 027<0567:POQEIP>2.0.CO;2.
Wetzel, P., Maier-Reimer, E., Botzet, M., Jungclaus, J., Keenlyside, N., Latif, M., 2006. Effects of ocean biology on the penetrative radiation in a coupled climate model. J. Clim. 19 (16), 3973–3987. http://dx.doi.org/10.1175/JCLI3828.1.